

The aftermath of the Carnian carbonate platform demise: a basinal perspective (Dolomites, Southern Alps)

LORENZ KEIM*·†, CHRISTOPH SPÖTL* and RAINER BRANDNER*

**Institut für Geologie & Paläontologie, Innrain 52, Leopold-Franzens-Universität Innsbruck, A-6020 Innsbruck, Austria (E-mail: lorenz.keim@uibk.ac.at)*

†*Amt für Geologie & Baustoffprüfung, Autonome Provinz Bozen, Eggenalerstr. 48, I-39053 Kardaun (BZ), Italy*

ABSTRACT

In the Dolomites of northernmost Italy the carbonate-platform growth came to a standstill late in the Early Carnian (Late Triassic). The response to this shutdown of shallow-water carbonate production in the interplatform basins is largely unknown because erosion has removed most of the soft basinal sediments, giving rise to today's scenic landscape of the Dolomites. Mapping in the central part of the Dolomites and newly available core material has recently revealed a well-preserved succession of basinal rocks within the Heiligkreuz Hospiz Basin (ital. Ospizio di Santa Croce Basin). In this paper, the regional depositional nature of arrested carbonate platform production is reconstructed by tracing its sedimentological record across the slope and into the basin. The uppermost St. Cassian Formation, the time-equivalent basinal rocks to the prograding carbonate platforms, is overlain by the Heiligkreuz Formation, whose basal succession was deposited in a restricted and oxygen-depleted environment immediately post-dating the platform demise. The succession consists mainly of mudrocks, marlstones, and peloidal packstones, with abundant low-diversity ostracod and pelecypod fauna and early diagenetic dolomite. C and O isotope values of the basal Heiligkreuz Formation, post-dating platform demise, average + 2.4 and – 2.4‰, respectively, and largely overlap the isotopic composition of St. Cassian carbonates. A shift toward slightly lower $\delta^{13}\text{C}$ values in the Heiligkreuz Formation may reflect incorporation of isotopically depleted C released during bacterial sulphate reduction in the Heiligkreuz sediments. Sedimentological, palaeobiological and geochemical indices suggest that near-normal marine conditions persisted long after the shutdown of shallow water carbonate-platform growth, although there are clear indications of severely reduced oxygen levels in the restricted Heiligkreuz Hospiz interplatform basin. The Early Carnian platform demise induced a distinct switch in the locus of carbonate production from the shallow-water platform and slope to the basin floor and a decrease in the availability of dissolved oxygen in the basinal waters. It is inferred that anoxia extended at least temporarily to the top of the carbonate slope, as indicated by the onlap of normal-marine mounds by dark marlstones of the basal Heiligkreuz Formation.

Keywords Anoxia, carbonate platform demise, Dolomites, environmental stress, Late Triassic, stable isotopes.

INTRODUCTION

Mid to Upper Triassic palaeogeometries of platform-to-basin transects are well preserved in the

Dolomites, Southern Alps (northern Italy). For more than a century this locality has been a classic area to study the temporal and spatial evolution of carbonate platforms (von Mojsisovics, 1879;

Leonardi, 1967; Bosellini, 1984; De Zanche *et al.*, 1993; Bosellini *et al.*, 1996; Gianolla *et al.*, 1998a). Most platform carbonates are pervasively dolomitized, but the coeval basinal rocks are minimally altered diagenetically (Scherer, 1977). Platform growth in the region came to a standstill during the Early Carnian (Julian) and a mixed siliciclastic-carbonate succession covered the platforms and former basins. The input of coarse siliciclastic material is generally known as the 'Raibl event' in the Southern Alps and the western Northern Calcareous Alps (Austria) and as 'Rein-graben' and 'Lunz event' in the eastern Northern Calcareous Alps (Schlager & Schöllnberger, 1974; Liebermann, 1979; Krystyn, 1998; Hornung & Brandner, 2005). Whether the platform demise resulted from burial beneath siliciclastic sediments or carbonate production terminated prior to the onset of siliciclastic sedimentation remains a topic of much debate. In addition, most of the carbonate platforms in the Dolomites and in the Northern Calcareous Alps became sub-aerially exposed because of a sea-level fall during early Carnian time (Bosellini, 1984; Brandner, 1984; De Zanche *et al.*, 1993, 2000; Gianolla *et al.*, 1998a).

Based on a sedimentological study of the Carnian Schilfsandstein in Germany and equivalent deposits in Great Britain, Simms & Ruffell (1989) postulated a 'pluvial event' which interrupted the general arid climate of the Late Triassic and led to enhanced run-off and accumulation of coarse, immature siliciclastics. This change to humid conditions at the Julian–Tuvanian boundary was further supported by sedimentological studies in the Dolomites (Gianolla *et al.*, 1998b; Preto & Hinnov, 2003; Stefani *et al.*, 2004) and in the Lombardian Alps (Berra & Jadoul, 2002), as well as by palynological studies of the Raibl Group in the eastern Swiss Alps (Hochuli & Frank, 2000) and of the Conzen and Tor Formations in the Julian Alps (Roghi, 2004). It is currently unclear, however, whether this climate shift was Tethyan-wide or even global in extent (Visscher *et al.*, 1994).

In the Dolomites, the sharp contrast in weathering relief between the high-standing carbonate platforms and the softer basinal rocks mimics the former sub-marine topography (Fig. 1A). The present-day landscape is biased toward the resistant shallow-water carbonate bodies as Quaternary erosion has removed most of the soft basinal rocks. Thus, the sedimentary evolution in the intervening basins after the Julian platform demise is poorly recorded.

Recent mapping in the central part of the Dolomites has allowed the spatial delineation of the sedimentological expression of the standstill in carbonate production from the platform and across the slope into the basin. This paper builds on a paper on slope and basinal deposits (Keim *et al.*, 2001), incorporating newly available core material (Fig. 1B and C). A variety of mineralogical and geochemical methods are utilized to examine well-preserved sample material in order to decipher the response of the basin to the termination of platform carbonate production during the Late Julian.

GEOLOGICAL SETTING

The Dolomites of the Southern Alps occupied a northern equatorial position (*c.* 16° N) in the western Tethys during Carnian time (Broglia Loriga *et al.*, 1999). During the Ladinian sedimentation took place on a passive continental margin associated with synsedimentary faulting and local mafic volcanism (e.g. Assereto *et al.*, 1977; Bosellini, 1984; Brandner, 1984; Castellarin *et al.*, 1988; De Zanche *et al.*, 1993; Bosellini *et al.*, 1996 and references therein). Isolated carbonate platforms, represented by the Schlern Dolomite, grew on structural highs whereas the surrounding deep basins were filled by platform- and slope-derived material, volcanics and erosional volcanoclastics. A decrease in subsidence following cessation of volcanic activity combined with pronounced lateral growth of the platforms and high input of clastic and platform-derived material resulted in basin aggradation. For the Carnian carbonate platforms, which interfinger with the basinal St. Cassian Formation (ital. *Formazione di San Cassiano*), the term 'Cassian Dolomite' is used (von Mojsisovics, 1879; Assereto *et al.*, 1977; Bosellini, 1984; De Zanche *et al.*, 1993). Some previous authors refer to this unit as the 'Upper Schlern Dolomite' (e.g. Biddle *et al.*, 1992; Keim *et al.*, 2001). The St. Cassian Formation consists of mudrocks, marlstones, micritic limestones, calcarenites and carbonate breccias and hosts a highly diversified, open-marine, pelagic fauna (Fürsich & Wendt, 1977; Wendt & Fürsich, 1980; Urlichs, 1994; Broglia Loriga *et al.*, 1999).

Carbonate production on the platforms and upper slopes came to a standstill in the Julian 2 and a mixed siliciclastic-carbonate succession covered the platforms throughout the entire Dolomites. Depending on the lithofacies,

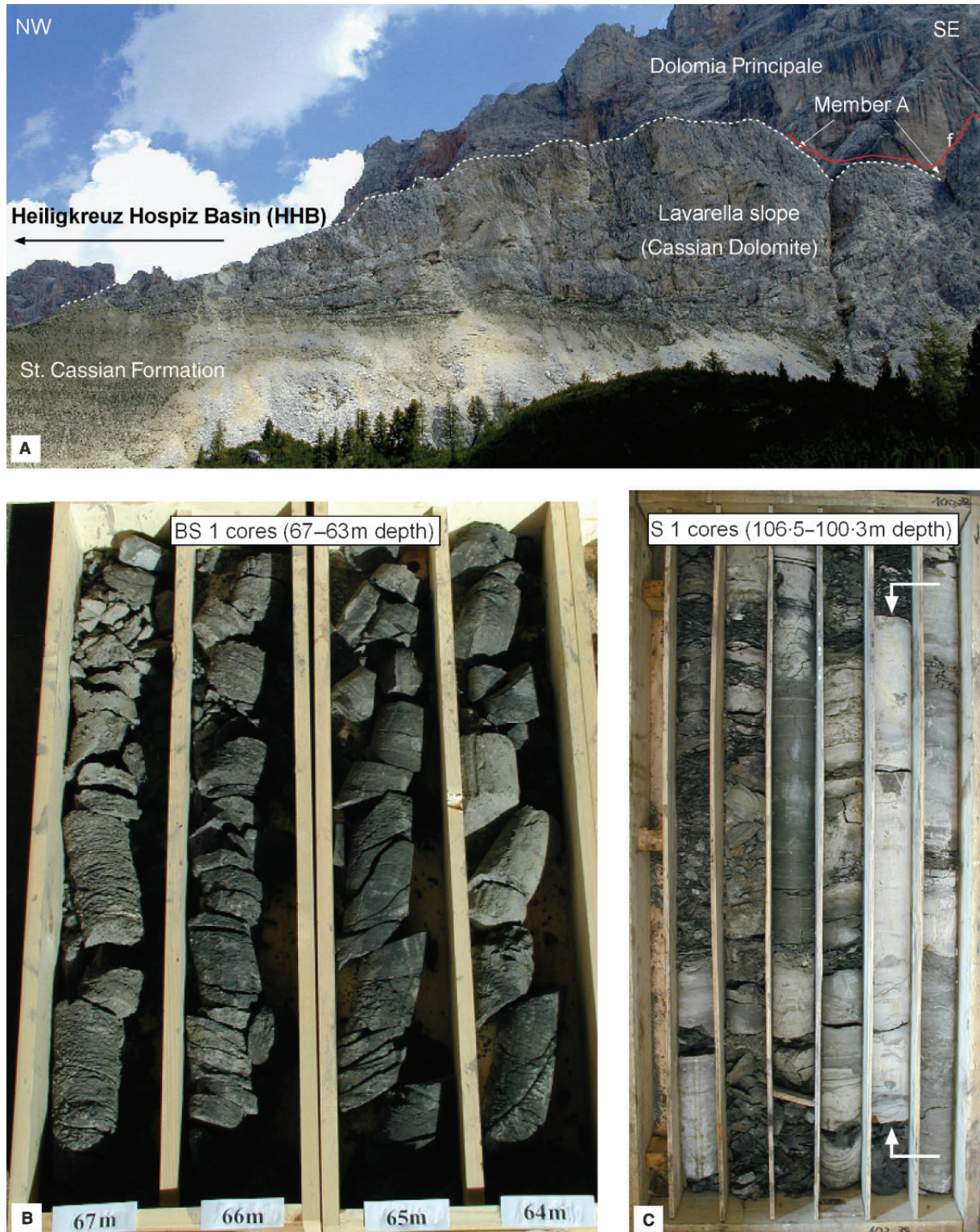


Fig. 1. (A) Panoramic outcrop view of the Lavarella palaeoslope in the central Dolomites. Note selective erosion between hard platform rocks and soft basinal rocks in foreground. Stippled line marks the top surface of the arrested carbonate slope. The Cassian Dolomite slope is covered by black marlstones, bioclastic packstones, and shell rudstones (member A), which is here a few metres thick only because of the down-faulted Dolomia Principale (f = normal fault). (B) Core material of the basal Heiligkreuz Formation (Member A) from BS1 borehole. Note the monotonous succession of dark mudrock and marlstone. (C) Core material of Member A from S1 borehole. Core segment S1-101 (between white arrows) was analysed in detail.

geographic location, and stratigraphic position, these mixed siliciclastic-carbonate deposits have been referred to as the 'Raibler Schichten' (von Mojsisovics, 1879) or 'Strati di Raibl' (Leonardi, 1967), 'Areniti del Dibona' (Bosellini *et al.*, 1982), Dürrenstein Formation (*sensu* De Zanche *et al.*, 1993; Gianolla *et al.*, 1998a,b; Preto & Hinnov, 2003) or Heiligkreuz Formation (Keim *et al.*, 2001; Stefani *et al.*, 2004), following Koken (1913) and Bosellini & Largaiolli (1965).

The Heiligkreuz Hospiz Basin

The mixed siliciclastic-carbonate deposits post-dating the platform demise are well exposed on the platform tops, but were largely removed by Quaternary erosion in the interplatform basins. The Heiligkreuz Hospiz Basin (HHB) in the central Dolomites (Fig. 2), however, preserves an exceptional depositional record of the Carnian carbonate platform demise and its aftermath. This interplatform basin – a remainder of the former extensive Cassin basin – is filled by dark, mud-rock-dominated sediments post-dating the platform demise (Heiligkreuz Formation).

An earlier paper (Keim *et al.*, 2001) documented the sedimentary response on a steep carbonate slope bordering this basin (Lavarella slope, Fig. 1A). This study focuses on the St. Cassian Formation at Lavarella (see Keim *et al.*, 2001) and in a newly measured section at Fedares and the basal Heiligkreuz Formation, which was studied in two drill cores (Fig. 1B and C). A few outcrops at the western foot of the Kreuzkofel/Sasso della Croce Massif in the eastern Gader/Badia valley of the Dolomites were also studied (Fig. 2A and B).

Stratigraphy

The lithostratigraphic units used in this paper comprise – in stratigraphic order – the St. Cassian Formation, the Cassian Dolomite, the Heiligkreuz Formation, and the Travenanzes Formation (all being Carnian in age, Fig. 3). Here the subdivision of the Carnian stage *sensu* Krystyn (1979) is used, who defined two sub-stages, the Julian (Early Carnian) and the Tuvallian (Late Carnian). Both sub-stages are, furthermore, subdivided, e.g. Julian 1, 2 (Fig. 3).

The St. Cassian Formation consists of basinal deposits adjacent to the prograding carbonate platforms of the Cassian Dolomite. In its upper portion, the St. Cassian Formation consists largely of calcarenites interlayered with brownish-grey marlstones (Figs 4 and 5). New conodont

data from the Fedares section indicate a Julian 1 age (= Aonoides Zone *sensu* Krystyn, 1979, see Fig. 3). The fauna includes *Gladigondolella tethydis*, branched forms of *Gladigondolella*, *Metapolygnathus polygnathiformis*, *M. auriformis* and *M. tadpole* (Fig. 4).

The basal Heiligkreuz Formation, which filled the HHB after the platform demise and subsequently spread out over the adjacent carbonate platforms (Fig. 2C), consists of mudrocks, marlstones, siltstones, sandstones, conglomerates, limestones and dolomites. The thickness of the Heiligkreuz Formation in the study area varies between about 140 m in the former basinal area and 30 m on the platform, reflecting the inherited palaeotopography (Fig. 2C).

The stratigraphic terminology used in this paper divides the Heiligkreuz Formation into four informal members, A–D (Figs 2C,D and 6).

Member A, the focus of this study, is poorly exposed and limited to the HHB, which is bordered to the south by the abandoned Lavarella palaeoslope (Fig. 2C). Scattered outcrops of Member A are located near the Heiligkreuz Hospiz/Ospizio di Santa Croce (Fig. 2B), some 700 m to the NNW, and about 2 km south of the Lavarella locality. Member A is dominated by organic-carbon-bearing mudrocks and marlstones with abundant shells of the bivalve *Unionites münsteri* (Wissmann), lime mudstones and wackestones, dolomudstones, peloidal micrites, and ostracod packstones and grainstones. This unit is in the order of 90 m thick although there is no continuous section. Distinct mm-scale lamination was observed in sub-surface exposures of member A in a water drainage tunnel near Heiligkreuz Hospiz/Ospizio di Santa Croce. Koken (1913) introduced the term 'Anoplophoraschichten' for this unit to underscore the abundant occurrence of the bivalve *Unionites münsteri* (Wissmann). 'Anoplophora' is the former, now obsolete name for *Unionites*. Additionally, member A is known for its abundant vertebrate remains in outcrop immediately southeast of the Heiligkreuz Hospiz/Ospizio di Santa Croce (Koken, 1913; Bizzarini & Rottonara, 1997; Dalla Vecchia & Avanzini, 2002; M. Urlichs, pers. comm., 2002). Based on the monotypic occurrence of *Unionites münsteri*, the mass occurrence of low-diversity ostracods, and the lack of diagnostic normal-marine biota, member A has been interpreted as a brackish-water deposit (Koken, 1913; Bizzarini & Rottonara, 1997; Keim *et al.*, 2001).

Member B crops out immediately east of Heiligkreuz Hospiz/Ospizio di Santa Croce

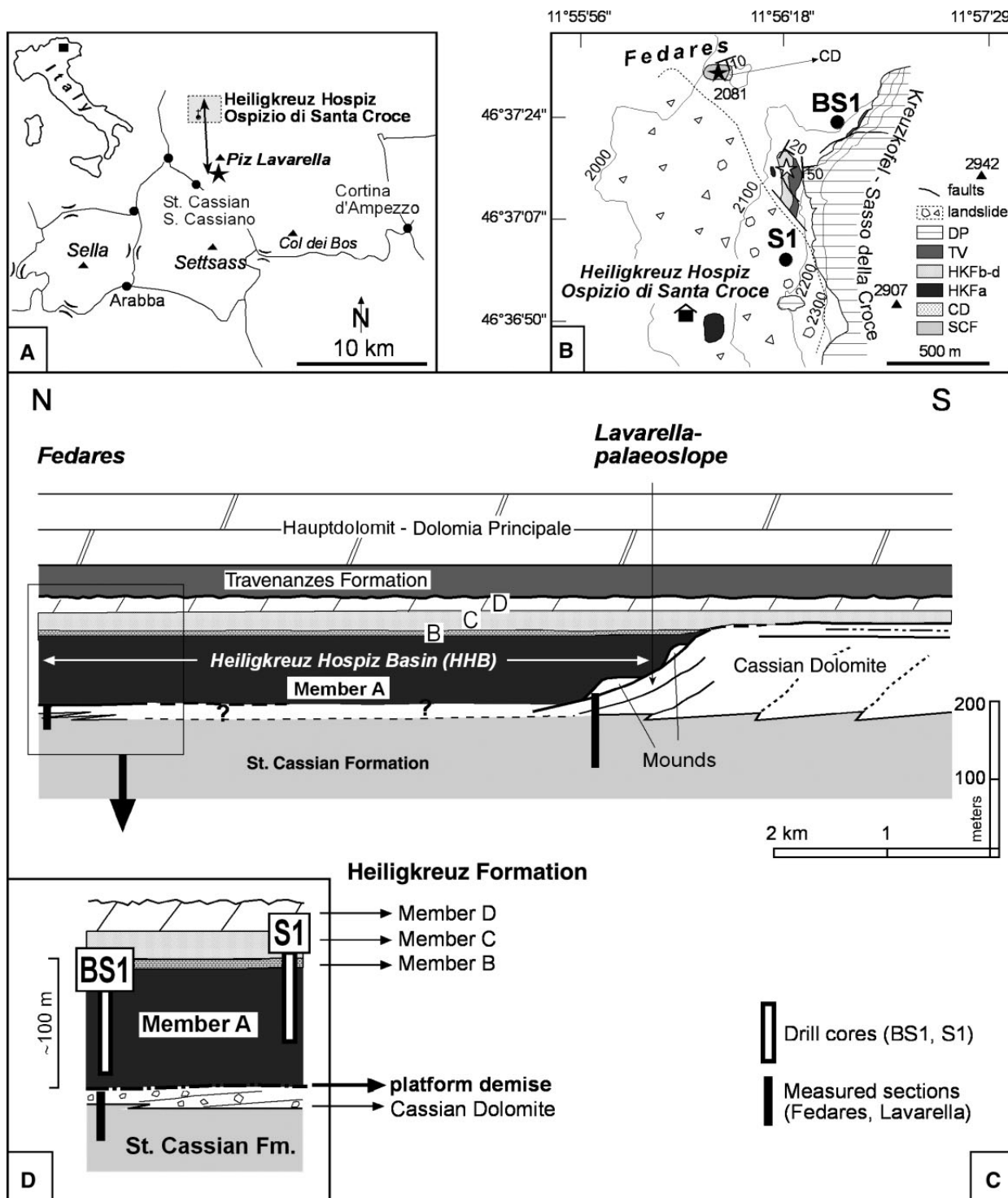


Fig. 2. (A) Location map (asterisk indicates position of Lavarella section – see Fig. 4). (B) Geological map of the Heiligkreuz Hospiz (Santa Croce) area (shaded rectangle in (A)). SCF, St. Cassian Formation; CD, Cassian Dolomite; HKFa, Heiligkreuz Formation: member A; HKFb-d, members B, C and D; TV, Travenanzes Formation; DP, Dolomia Principale. Solid and open asterisks indicate locations of measured sections in the St. Cassian and the Heiligkreuz Formations respectively (see Figs 4 and 6). (C) Schematic cross-section along the arrow in (A). (D) Stratigraphic location of the drill cores. For discussion of the lithostratigraphy see text. Note distinct difference in thickness of the Heiligkreuz Formation between the HHB (c. 140 m) and the platform (< 50 m) and the pinch-out of member A onto the Lavarella palaeoslope.

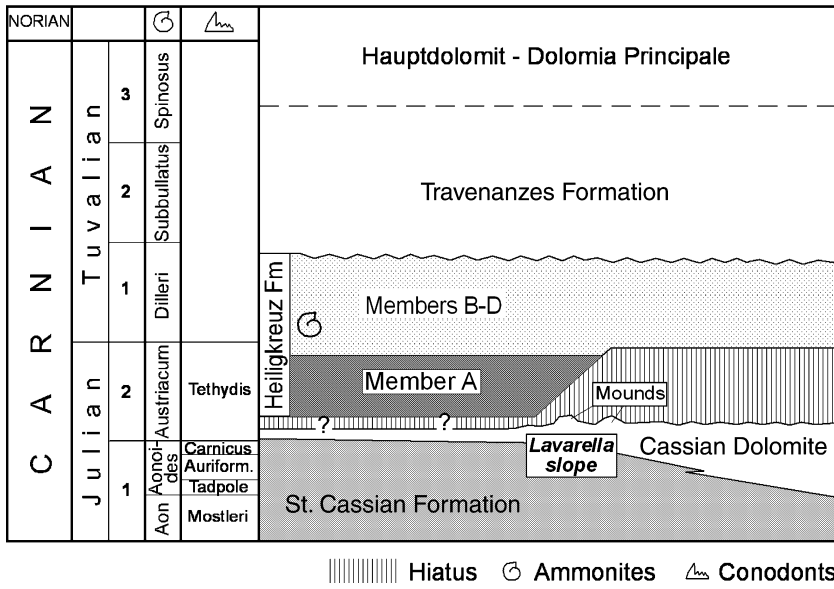


Fig. 3. Chronostratigraphic framework of the study area based on De Zanche et al. (1993), Gianolla et al. (1998b), De Zanche et al. (2000), Keim et al. (2001), Stefani et al. (2004) and the present work.

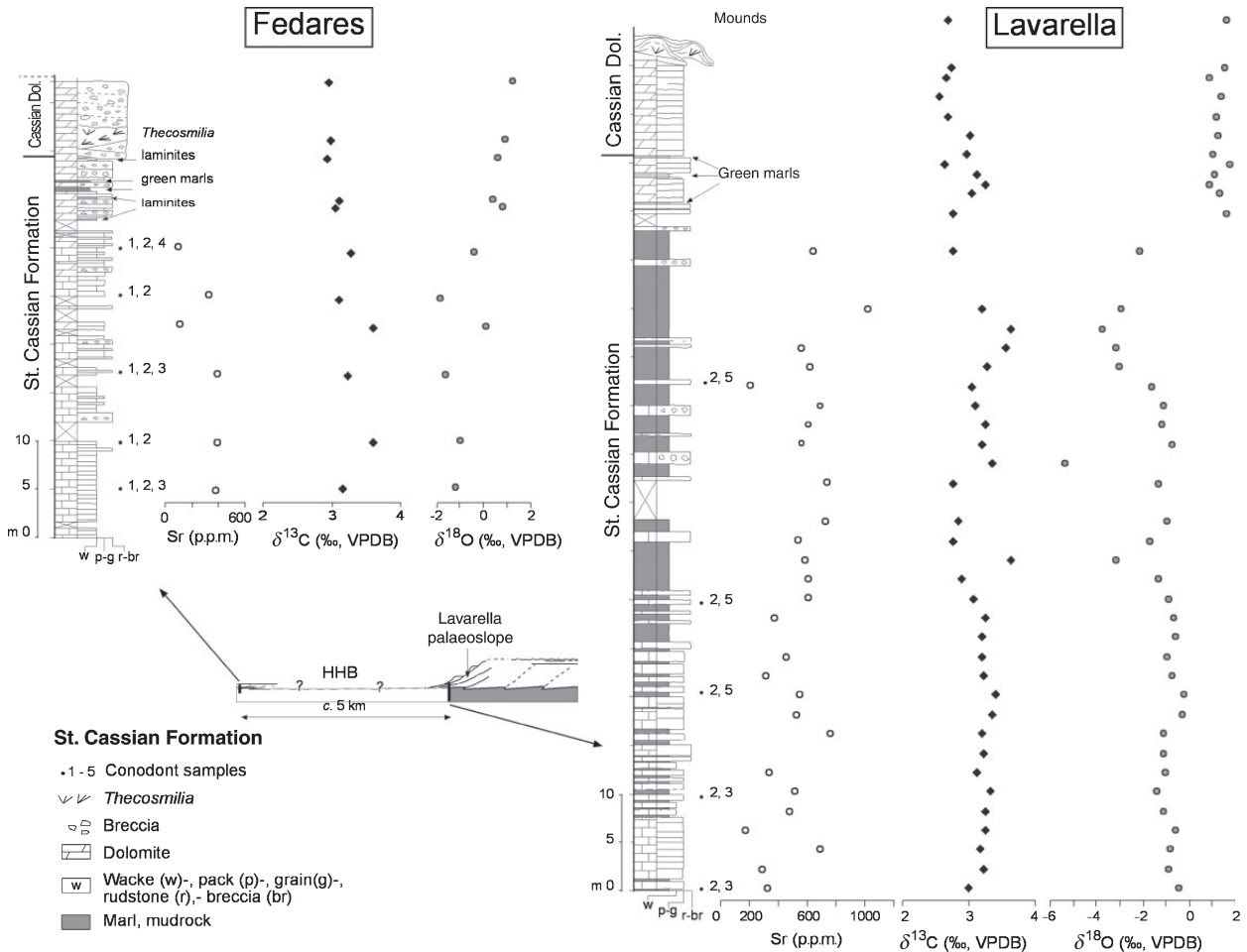


Fig. 4. Lithological sections of the uppermost St. Cassian Formation at Fedares and Lavarella (for location see Fig. 2B), conodont samples, Sr contents and stable C and O isotope data. Arrows indicate position of green marl layers, which were used as correlation marker beds between the two sections. Note the higher oxygen isotope values in the upper, dolomitic part of both sections. HHB, Heiligkreuz Hospiz Basin. Conodont samples: 1 = *Gladigondolella tethydis*, 2 = *Metapolygnathus polygnathiformis*, 3 = *Metapolygnathus auriformis*, 4 = *Metapolygnathus tadpole*, 5 = *Gladigondolella malayensis*.

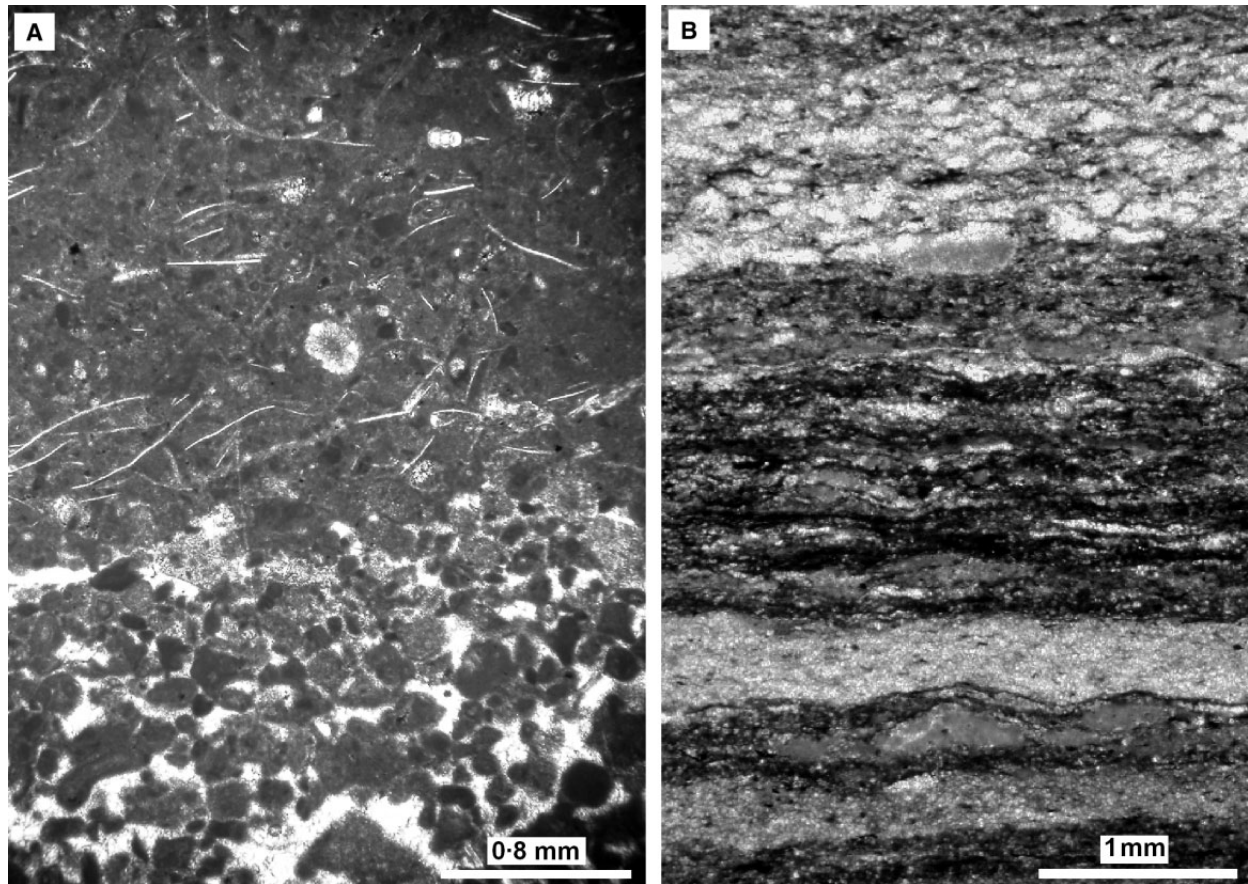


Fig. 5. (A) Thin-section photomicrograph of the St. Cassian Formation at Fedares. Graded bed consisting of a peloidal and lithoclastic rudstone passing upward into a wackestone with thin-shelled bivalves. (Sample HK1, at 9 m in the section, see Fig. 4). (B) Distinct alternation of very fine-grained calcarenite (light) and wavy, micritic layers (brownish and dark grey) from the topmost part of the St. Cassian Formation (Fig. 4, arrows). Absence of bioturbation as well as the presence of pyrite indicates an oxygen-depleted environment (Sample FS 35b).

(‘oolithische Kalkplatte’ of Koken, 1913) as well as 2 km south of it (basal interval of the section in Gianolla *et al.*, 1998b, ‘interval B’ in Keim *et al.*, 2001). It is up to 10 m thick (in the S1-core section), and is composed primarily of calcarenites, including oolitic and peloidal grainstones with low-angle cross-bedding, bioturbated wackestones, and a fenestral dolomite bed 0.5 m thick on top. Member C, whose thickness varies between 15 m (at Fedares, Fig. 6) and *c.* 50 m further to the south-east, is made up of conglomerates, siltstones, sandstones, marlstones, bivalve coquinas, wackestones, packstones and dolostones. Member D, up to 20 m thick, consists of cross-bedded oolitic grainstones at the base, bird’s-eye dolostones, and sub-tidal dolostones. Members b–d have been previously interpreted as largely a marginal-marine environment with tempestites, tidal-flat sedimentation, intermittent sub-aerial exposure (Gianolla *et al.*, 1998b; Keim *et al.*, 2001) and repeated palaeosol formation

(Preto & Hinnov, 2003). Preto & Hinnov (2003) postulated a ramp setting during deposition of the Heiligkreuz Formation (their ‘Dürrenstein Formation’ A–D) in the surroundings of Cortina d’Ampezzo, located several kilometres southeast of the study area.

The succession above the Heiligkreuz Formation is herein termed Travenanzes Formation following Bosellini *et al.* (1996, their ‘Argilliti di Travenanzes’) and corresponds to the Raibl Formation *sensu* De Zanche *et al.* (1993). Breccias at the base of the Travenanzes Formation overlie erosional incisions on the top of member D of the Heiligkreuz Formation (Fig. 6). These incisions are locally several metres deep. The Travenanzes Formation consists of variegated marlstones and aphanitic dolostones interpreted as tidal-flat and sabkha facies (Bosellini *et al.*, 1996).

The age of the Heiligkreuz Formation is well constrained by ammonoid and palynomorph

Heiligkreuz Hospiz Basin

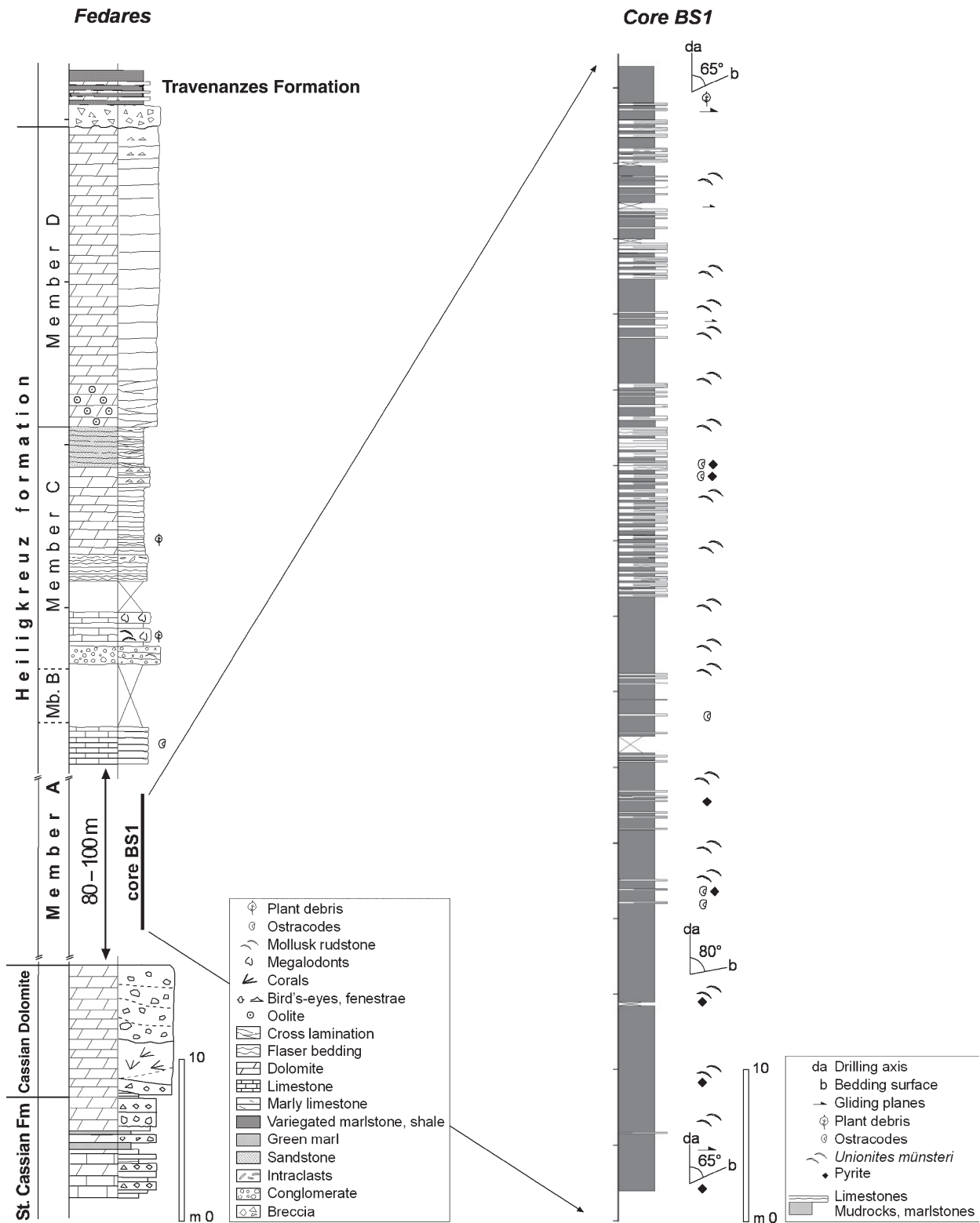


Fig. 6. Composite section of the Carnian succession north of Heiligkreuz Hospiz/Ospizio di Santa Croce composed of two outcrop sections (see Fig. 2B for location) and core BS1. Note different scales.

findings by Gianolla *et al.* (1998b) and De Zanche *et al.* (2000) and spans the Julian–Tuvalian boundary (Austriacum and Dilleri Zones; Fig. 3).

SAMPLE MATERIAL AND METHODS

The data presented are based on field mapping, measured sections, and drill cores S1 and BS1, which are located 700 m apart (Fig. 2B–D). Surface samples of the St. Cassian Formation from the Fedares and Lavarella sections were examined petrographically and geochemically. Samples of the basal unit of the Heiligkreuz Formation (member A) were studied in drill cores S1 and BS1. S1 was drilled in 1998 so as to determine the glide planes of the Kreuzkofel land slides (Fig. 2B). The second core, BS1, was drilled in 2001 for scientific purpose. Unfortunately, neither of the drill holes penetrated the base of member A. Based on the average dip at the top of the St. Cassian Formation and the Cassian Dolomite at Fedares (Fig. 2B) it is estimated that the uncored interval of member A of the Heiligkreuz Formation is 10–30 m thick.

Borehole S1 was drilled between 2176 and 2025 m, and penetrated the basal conglomerates of member C below about 73 m of Quaternary rubble and blocks (Fig. 2D). A total interval of 78 m was cored within the basal Heiligkreuz Formation (members A and B, and ~2 m of member C). The true stratigraphic thickness, however, may be slightly less, because of the dip of the strata (on average < 15°) and because of the presence of several gliding planes. One representative carbonate interval of core S1 of 75 cm length (from 101.44 to 102.19 m), hereafter referred to as S1-101, was analysed in detail. Borehole BS1 was drilled at 2093 m altitude and penetrated 76 m of member A below 28 m of Quaternary cover (Figs 2D and 6). The true stratigraphic thickness is somewhat less reflecting structural dip. Core recovery was rather poor in BS1 because of technical difficulties. The stratigraphic overlap between S1 and BS1 is *c.* 40 m (Fig. 2D). All cores were slabbed; one half was used for thin-section preparation and the other half for geochemical analyses. The fine grain size of the limestones and dolostones precluded physical separation of individual components. Thus, all geochemical data refer to whole-rock analyses.

Thin sections were examined using a standard polarizing microscope equipped with a UV/blue-light epifluorescence unit. A Technosyn MK II cold-cathode device operating at an accelerating voltage of 18 kV and 500 mA beam current was

used for cathodoluminescence (CL) microscopy. Selected polished thin sections were also examined in back-scattered electron (BSE) mode using a low-vacuum scanning electron microscope (SEM). Mineral identification was facilitated using an energy-dispersive X-ray analytical system (EDS). X-ray diffraction (XRD) analyses of samples taken at 1 cm intervals were performed on a Siemens D500 diffractometer using Ni-filtered CuK α radiation, 30 kV voltage, 38 mA, 2–100° 2-theta scan range, 0.02° 2-theta step interval, and 5 sec integration time per step. Using these data, crystal parameters were refined using the Rietveld software SIROQUANT (Taylor, 1991). Following background subtraction the following parameters were refined: instrument zero point, scale factors, line asymmetry, preferred orientation, phase line widths (U, V, W) and line shape. Most samples contained small amounts (< 5%) of illitic clay minerals, which were not included in the refinement process. Calcite and dolomite composition (stoichiometry) were calculated from the unit-cell dimensions directly obtained by SIROQUANT refinements (Taylor, 1991). In addition, the software calculates relative weight percentages of calcite and dolomite (Bish & Post, 1993; Ward *et al.*, 1999).

Calcite-rich samples (> 87 wt% calcite according to quantitative XRD analyses) were dissolved in 65% suprapure nitric acid and the concentrations of Mg and Sr were determined using a Philips PU 7000 inductively coupled plasma optical emission spectrometer. Merck standard solutions were used to calibrate the machine. Precision (1 σ) at the measured levels of concentrations is 5% for each element.

Stable isotope analyses were performed on both calcite-rich samples (> 90 wt% calcite according to quantitative XRD analyses) and dolomite-rich samples (> 70 wt% dolomite; no attempt was made to remove calcite prior to analysis). Seventy-seven calcite samples were taken over the entire 76 m of core BS1. In addition, detailed samples at *c.* 5 mm-intervals were obtained from the S1-101 core segment (*n* = 116) so as to investigate compositional variability at high-resolution. Calcite and dolomite samples were drilled from the slabs using a dental drill. Carbonate powders were reacted with concentrated phosphoric acid at 72 °C (calcite) and 90 °C (dolomite), respectively, using a Thermofinnigan (Bremen, Germany) GasBench II and the evolved gas was analysed using a Delta^{plus}XL mass spectrometer. Calcite samples were calibrated against VPDB using an in-house marble standard

(corrected to NBS 18 and NBS 19), and dolomite samples were calibrated against a dolomite standard (corrected for the phosphoric acid fractionation factor) provided by T. Vennemann, University of Lausanne. The analytical error (1σ) for $\delta^{13}\text{C}$ and $\delta^{18}\text{O}$ is 0.07 and 0.08‰, respectively (Spötl & Vennemann, 2003).

Clay mineralogy of Member A mudrock samples ($n = 8$) was determined by XRD analysis of the $< 2 \mu\text{m}$ fraction by $\text{CuK}\alpha$ radiation; analysis was carried out on air-dried samples subsequently saturated with ethylene glycol, and then heated to 550 °C. The total-carbon (C_{tot}), sulphur (S), and organic-carbon (TOC) contents were determined on a suite of mudrocks, marlstones and dolostones using a LECO 300 CS TM analyzer (LECO Instrumente GmbH Mönchengladbach, Germany). The ground powder was treated with 2 N HCl acid before measurement to isolate the acid insoluble fraction. Rock-Eval pyrolysis measurements were performed using standard techniques (Peters, 1986).

SEDIMENTOLOGY AND PETROGRAPHY

St. Cassian Formation

The lithofacies of the St. Cassian Formation at Lavarella have been described by Masetti *et al.* (1991) and Keim *et al.* (2001). Here, a newly measured section at Fedares, located *c.* 1 km west of borehole BS1 is presented (Fig. 2B). The exposed St. Cassian Formation is about 40 m thick and is covered by the Cassian Dolomite (Fig. 4). The lower part consists predominately of wackestones (up to 40 cm thick) with abundant thin-shelled bivalves, and locally dolomitized packstones and grainstones, all separated by marl seams. Graded beds are common; peloidal packstones or grainstones at the base pass upward into wackestones with thin-shelled bivalves (Fig. 5A). Above 13 m in the section, packstones, grainstones, rudstones and breccias dominate. The thickness and frequency of breccias, which are commonly dolomitized, increases upsection (Fig. 4).

Above 35 m in the section, the lithology changes to an alternation of fine-grained, laminated wackestones and packstones (up to 10 cm thick), green mudrocks and marlstones, marly dolostones, grainstones, rudstones, and breccias. Some of the breccia beds have an erosive base. Millimetre-to-centimetre-sized plant fragments are common at the base of the rudstones.

In thin-section, the fine-grained laminites show alternations of light- and brownish-coloured, layers (Fig. 5B). The light-coloured layers consist of silt to fine sand-size skeletal and lithoclastic wackestones and packstones that are commonly graded. Skeletal grains include thin-shelled bivalves and the foraminifera *Dendrophrya*. The brownish-coloured layers consist of wavy, sub-millimetre, micritic layers (Fig. 5B). The brownish colour is caused by pyrite that is locally altered to Fe-oxides. Such micritic layers are absent in stratigraphically deeper positions of the St. Cassian Formation.

Breccias from the uppermost St. Cassian Formation (between 33 and 40 m) form beds 10–30 cm thick. Breccia components range up to 10 cm in diameter and consist of completely dolomitized or recrystallized lithoclasts and bioclasts (e.g. rare red algal clasts). Strongly recrystallized clasts, typically a few centimetres in size, are codiacean (green algae) detritus. Most of the codiacean clasts exhibit geopetal fills of fine-grained sediment in upright position, indicating that infiltration and recrystallization post-date clast deposition.

The Cassian Dolomite at the top of the section, *c.* 8 m thick (top missing), consists largely of breccias separated by a *Thecosmilia* coral bank, which is 2 m thick (Fig. 4). Bed thickness of the breccias is 50–80 cm. Most of the *Thecosmilia* corals are in growth position. The base of the *Thecosmilia* bank is at an angle of about 15° relative to the breccia bedding below (Fig. 4). Some hundreds of metres SW of Fedares, however, the Cassian Dolomite is directly overlain by centimetre-bedded, dark, bituminous lime mudstones of Member A of the Heiligkreuz Formation.

Heiligkreuz Formation (member A)

Member A can be sub-divided into the following facies types: (1) mudrocks and marlstones with organic matter; (2) lime mudstones, wackestones and dolomudstones; and (3) peloidal and ostracod packstones, and, rarely, grainstones.

Mudrocks and marlstones

The mudrocks and marlstones form intervals a few centimetres to several metres thick, that comprise 50–60% of the BS1 and S1 cores. The term ‘mudrock’ is used here for non-calcareous or calcareous sediments with up to 50 wt% CaCO_3 , because core samples lack the typical fissility of shales.

Fine-grained, disseminated pyrite is present throughout this unit (Fig. 6). No macroscopic sedimentary structures were observed. The mudrocks and marlstones contain abundant thin-shelled, brown-coloured, monospecific bivalves (*Unionites münsteri*), which form distinct shell beds a few centimetres thick (Fig. 7A). The valves are of uniform size, are well preserved and lack abrasion or fragmentation. XRD analyses of hand-picked shells show that they consist predominantly of aragonite (c. 80%) with both high-Mg and low-Mg calcite. The mudrocks and marlstones also contain abundant ostracods, mostly low-diversity occurrences dominated by *Renngartenella santaecrucis* (locus typicus Heiligkreuz; Kristan-Tollmann & Hamedani, 1973) and *Simeonella brotzenorum nosterica*. *Bairdia* sp., *Bairdiacypris*? sp., *Kerocythere* cf. *sulcata*, *Reubenella* cf. *avnimelechi* and *Reubenella* sp. were also detected. These species are filter-feeding podocypids. In addition, bivalves, gastropods, e.g. *Ampullina santaecrucis* (Wissmann) and *Ampullina paludinaris* (Münster), and vertebrate remains are present (mainly teeth from fishes and Crocodylomorpha, see Bizzarini & Rottonara, 1997; Dalla Vecchia & Avanzini, 2002).

Lime mudstones, wackestones and dolomudstones

Lime mudstones and wackestones form layers a few centimetres to 80 cm thick. Primary bedding is frequently overprinted by pressure-solution seams. The mudstones and wackestones are composed of dense, structureless micrite, carbonate lithoclasts, pyritized grains and rare skeletal grains. Most of the sediment is bioturbated. Dolomudstones form either distinct individual layers interbedded with lime mudstones and wackestones (Fig. 7B) or very irregularly distributed, diffuse seams within mudstone or wackestone beds.

Petrographically, dolomudstones consist of euhedral dolomite rhombs mostly in contact with organic matter. Both the mud-supported limestones and the dolomudstones contain swarms of anastomosing dissolution seams composed of insoluble residue of organic matter and clay minerals (the non-sutured seams of Wanless, 1979) (Fig. 7B). Dissolution seams wrap around allochems and form a fitted fabric of fissile limestones *sensu* Bathurst (1987).

Lime mudstones and dolomudstones have uniformly bright yellow–orange and reddish CL respectively.

Peloidal and ostracod packstones and grainstones

These carbonate facies are closely interrelated and form light-coloured limestone layers up to 20 cm thick within member A. The contacts to the aforementioned facies are sharp, enhanced by pressure solution (Fig. 7C). Bioturbation is common. Unbioturbated beds have millimetre- to centimetre-scale wavy layering consisting of alternating ostracod-rich peloidal layers and layers rich in clay, organic matter, and ostracods (Fig. 7C–F). The peloids occur both as discrete layers of fine-grained, well-sorted, commonly pyritized pellets, locally associated with black pebbles, and within layered and welded, clotted textures containing spar-filled cavities (Fig. 7C–F). Occasionally, dense micritic crusts with bored surfaces are present (Fig. 7E).

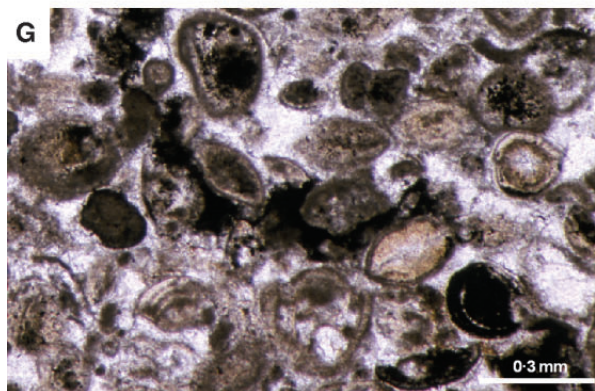
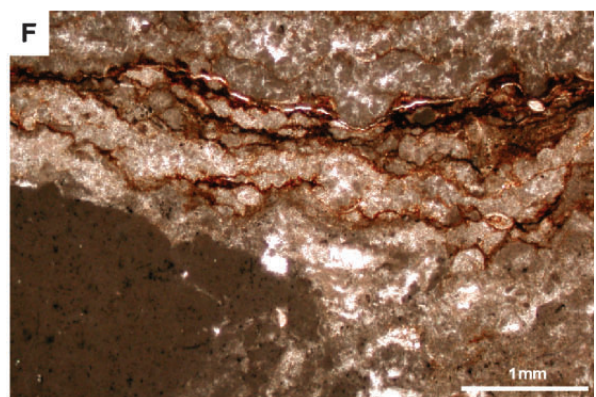
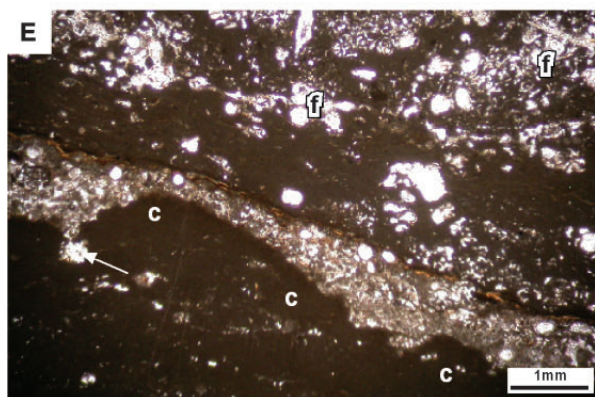
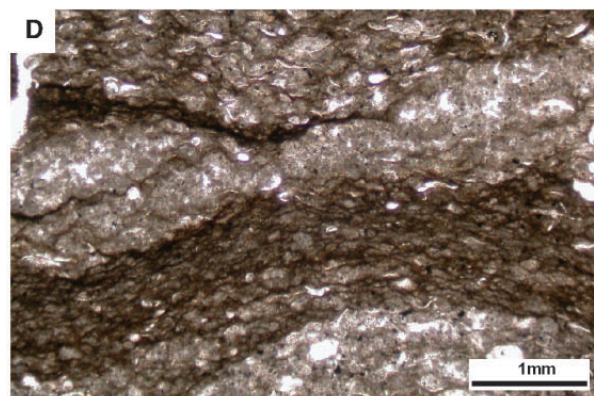
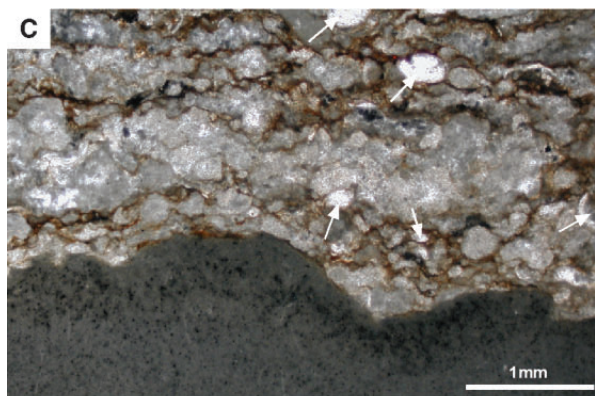
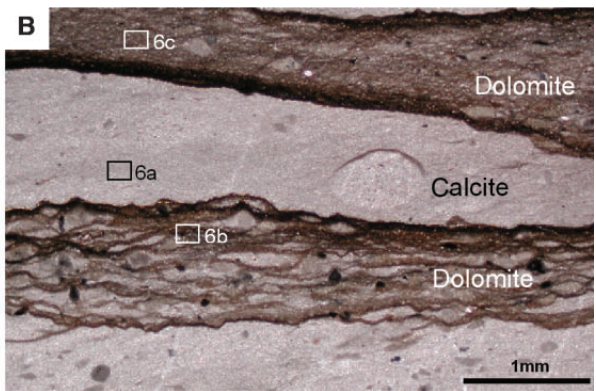
The peloidal packstone layers are about 0.5–3 mm thick and are separated by thin seams of insoluble residue forming brownish to dark organic-rich layers (Fig. 7C–E) or by layers of black, finely crystalline dolomudstones. These seams branch and wrap around peloidal clots and ostracods. The dissolution seams are mostly devoid of dolomite rhombs. Locally, ostracod grainstone layers with cement-filled pore space are present (Fig. 7G). Some ostracods are blackened and fragmented (Fig. 7G).

All facies types show rather homogeneously bright CL. The clotted, peloidal layers show a bright brownish-yellow epifluorescence, whereas the dense micritic crusts (Fig. 7E) are only weakly fluorescent. The cement-filled cavities within the layers of clotted peloids, ostracods, black peloids and black pebbles, as well as the thin dissolution seams, are non-fluorescent.

MINERALOGY AND GEOCHEMISTRY

Composition of carbonate rocks (member A, core segment S1-101)

X-ray diffraction analysis indicates that calcite and dolomite are the dominant mineral phases of the carbonate fraction in core segment S1-101. No aragonite is present. Illite-smectite mixed-layer minerals comprise < 5 wt% in a few samples. Pyrite is below XD detection limit, but has been identified in thin section by BSE microscopy and EDS analysis (Fig. 8). Calcite is present in all samples ranging from 10 to 100 wt%, whereas dolomite accounts for 0–90 wt% (Fig. 9).



Energy-dispersive X-ray analytical system analysis show that the calcite is essentially non-ferroan and compositionally homogeneous (Fig. 8A). Rietveld analysis reveals that calcite contains *c.* 3 mol% MgCO₃ (i.e. low-Mg calcite; Table 1). Dolomite forms euhedral rhombs, typically 5–30 µm wide, which are unzoned (BSE mode – Fig. 8B and C) and show a small Fe peak in the EDS spectrum. The crystal structure of dolomite deviates significantly from that of stoichiometric dolomite. The unit-cell dimensions of dolomite obtained from Rietveld refinements are consistently larger than those of stoichiometric dolomite (Table 2). Although substitution of ferrous Fe in the Mg site of the dolomite crystal structure will also give rise to an expanded unit cell (Reeder & Dollase, 1989), the measured values are much too large to be attributed to this effect only. If it is assumed that all the lattice expansion reflects Ca substitution, the data indicate non-stoichiometric dolomite with an overall composition of approximately 55 mol% CaCO₃ (Table 2).

Trace elements

St. Cassian Formation

Both the Fedares and Lavarella sections have been analysed for their Sr contents (Fig. 4). At Fedares, Sr values of six samples range from 99 to 404 p.p.m. with a mean of 291 (± 121) p.p.m. At Lavarella Sr values of 27 samples of wackestones, packstones and grainstones range from 178 to 1026 p.p.m. with a mean of 540 (± 188) p.p.m.

Heiligkreuz Formation (member A, core segment S1-101)

The Sr content of 50 calcite samples ranges between 159 and 600 p.p.m., except for 1 value

of 1016 p.p.m. (Fig. 10). The average of all values is 305 p.p.m. All lime mudstones and wackestones have Sr contents of about 300 p.p.m. A sharp lithological change at 49 cm to peloidal and ostracod packstones is accompanied by a distinct shift to higher Sr values between 433 and 1016 p.p.m. (Fig. 10).

The Mg content varies between 0.4 and 2.8 wt% (Fig. 10). The Mg content correlates positively with weight per cent dolomite (0–12 wt%) of calcite-rich samples. The Mg values were therefore corrected for the amount of dolomite in these mixtures, based on (a) the weight percentage dolomite derived from Rietveld refinements, and (b) the slightly Mg-depleted composition of this dolomite obtained from unit-cell dimensions (see above; Fig. 10). Resulting Mg values of the dolomite-free calcite show a gradual decrease from *c.* 1.4 to 0.4 wt% in the lower lime mudstones and wackestones, followed by a return to higher and more variable values above the peloidal packstone layer (above 57 cm – Fig. 10).

Stable isotopes

St. Cassian Formation

Eleven samples from the Fedares section have δ¹³C values between +3.1 and +3.6‰ with a mean of +3.3‰. The mean δ¹⁸O value is –0.6‰ with a range of –1.8 to +0.8‰ (Fig. 4). At the Lavarella section, δ¹³C and δ¹⁸O values range from +2.8 to +3.6‰ (mean +3.2‰) and from –0.2 to –6.2‰ (mean –1.8‰) respectively. In both localities the carbon isotope values are near invariant, whereas the oxygen isotope values are more variable. The abrupt shift in δ¹⁸O toward higher values at 70 m in the Lavarella section is associated with the presence of variable amounts of dolomite (Fig. 4).

Fig. 7. Lithofacies types of member A (basal Heiligkreuz Formation). (A) *Unionites münsteri* shell beds (BS1 core). All valves are oriented convex-up. Note also preservation of aragonite shells (core diameter = 8 cm). (B) Photomicrograph of the basal part of core segment S1-101 (see Fig. 1C). Alternation of lime mudstones, dominated by calcite, and dolomudstones containing organic carbon. Bedding planes are overprinted by pressure solution seams. Rectangles indicate positions of photomicrographs of Fig. 8. (C) Thin-section photomicrograph showing the alternation of black mudrock and ostracod-bearing, peloidal packstone. White arrows show individual ostracod shells within the peloidal layer. Note fitted fabric within the peloidal layers. (Sample S1-106.46 m) (D) Superposition of ostracod-rich packstones and layer of clotted peloids. Note the presence of residual organic matter within the ostracod-rich layers. (Sample BS1-33.5 m). (E) Dense micritic layer (c) with distinct relief on the upper surface, which has been bored (arrow). The micritic layer is interpreted as lithified upon formation. The overlying layers consist of skeletal, foraminifera-rich (f) packstone (Sample BS1-37.5 m). (F) Close-up view of peloidal layer showing clotted, microcolumnar textures (at the top of the picture). Dark mudrock at the lower left side. (Sample S1-106.46 m). (G) Photomicrograph of an ostracod grainstone. Note locally broken shells as well as local blackening of the ostracod shells. (Sample BS1-33.5 m).

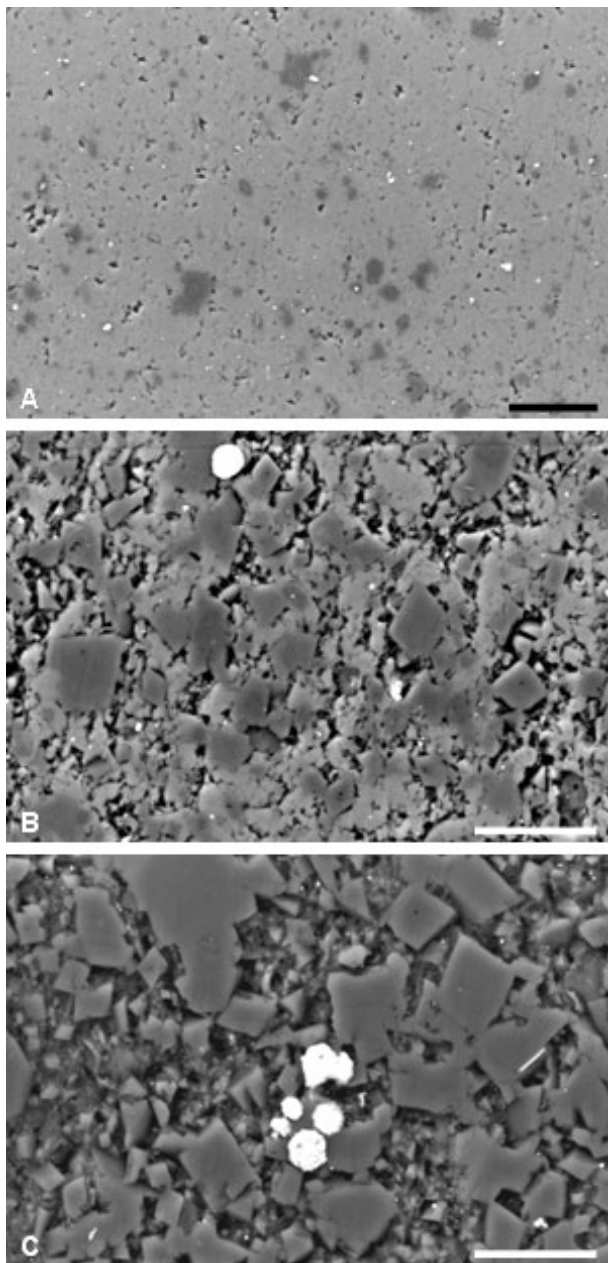


Fig. 8. Back-scattered electron micrographs of carbonate rocks of member A (for location see Fig. 7B): (A) typical lime mudstone containing traces of dolomite. (B) Euhedral dolomite rhombs (dark grey crystals) embedded in a calcitic matrix, (C) calcite-free dolospar and framboidal pyrite (white aggregates). Scale bars 50 μm .

Heiligkreuz Formation (member A)

Two sets of stable isotope data were obtained from member A. A reconnaissance study of 77 samples covered the entire length of core BS1 (76 m), and a detailed data set was developed for core segment S1-101 (116 samples from 75 cm core length, Fig. 9). The $\delta^{13}\text{C}$ values of BS1 vary between -0.5 and $+4.2\text{‰}$ (mean $+2.4\text{‰}$) and the

$\delta^{18}\text{O}$ values between -3.8 and $+0.2\text{‰}$ (mean -2.4‰ , see Fig. 11).

The $\delta^{13}\text{C}$ and $\delta^{18}\text{O}$ calcite values from the S1-101 core segment plot within the array defined by the reconnaissance data set of the entire core BS1 (Figs 9 and 11). Both the $\delta^{13}\text{C}$ and $\delta^{18}\text{O}$ values from S1-101 show rather constant values between $+1.1$ and $+2.5\text{‰}$ (mean 2.0‰) and -2.3 and -1.3‰ (mean -1.7‰ ; Figs 9 and 11). Eight dolomite samples define a limited range of $\delta^{13}\text{C}$ values from $+1.8$ to $+2.8\text{‰}$ and $\delta^{18}\text{O}$ values from $+0.6$ to $+1.7\text{‰}$ (Fig. 9). These samples contain up to 30 wt% calcite (which is depleted in ^{13}C and ^{18}O relative to the dolomite, Fig. 9) and, therefore, the dolomite values must be regarded as minimum values. Isotope values of *Unionites münsteri* shells (c. 80% aragonite – see above) have $\delta^{13}\text{C}$ values between $+1.1$ and $+3.2\text{‰}$ and $\delta^{18}\text{O}$ values between -1.9 and -1.3‰ (Fig. 11).

Clay mineralogy (member A)

The $< 2 \mu\text{m}$ fraction of five mudrock samples from drill core BS1 consists almost entirely of smectite. In contrast, thin mudrock seams (5 samples) within, beneath, and above the S1-101 core segment (see Figs 1C and 9) are dominated by illite and illite-rich illite-smectite mixed-layer minerals (five samples). Other clay minerals were not observed in XRD patterns.

Organic matter (member A)

Total organic-carbon values of samples from both cores vary between 0.2 and 0.9 wt% (Table 3). The values are higher in the mudrocks and marlstones than in the carbonates. Rock–Eval pyrolysis yielded hydrogen indices (HI) between 4.3 and 67.6 suggesting kerogen type III. Two samples have HI indices of 163.6 and 377, and thus plot in the field of immature kerogen type II (Fig. 12). The sulphur contents average between 0.06 wt% for carbonates and 1.4 wt% for mudrocks. $C_{(\text{org})}/S$ ratios are low (average 0.96, see Table 3) and plot in the marine field (Bernier & Raiswell, 1984).

DISCUSSION

From open-marine to basin restriction: the sedimentological response

The compositional variation from the St Cassian Formation to the overlying Heiligkreuz Formation

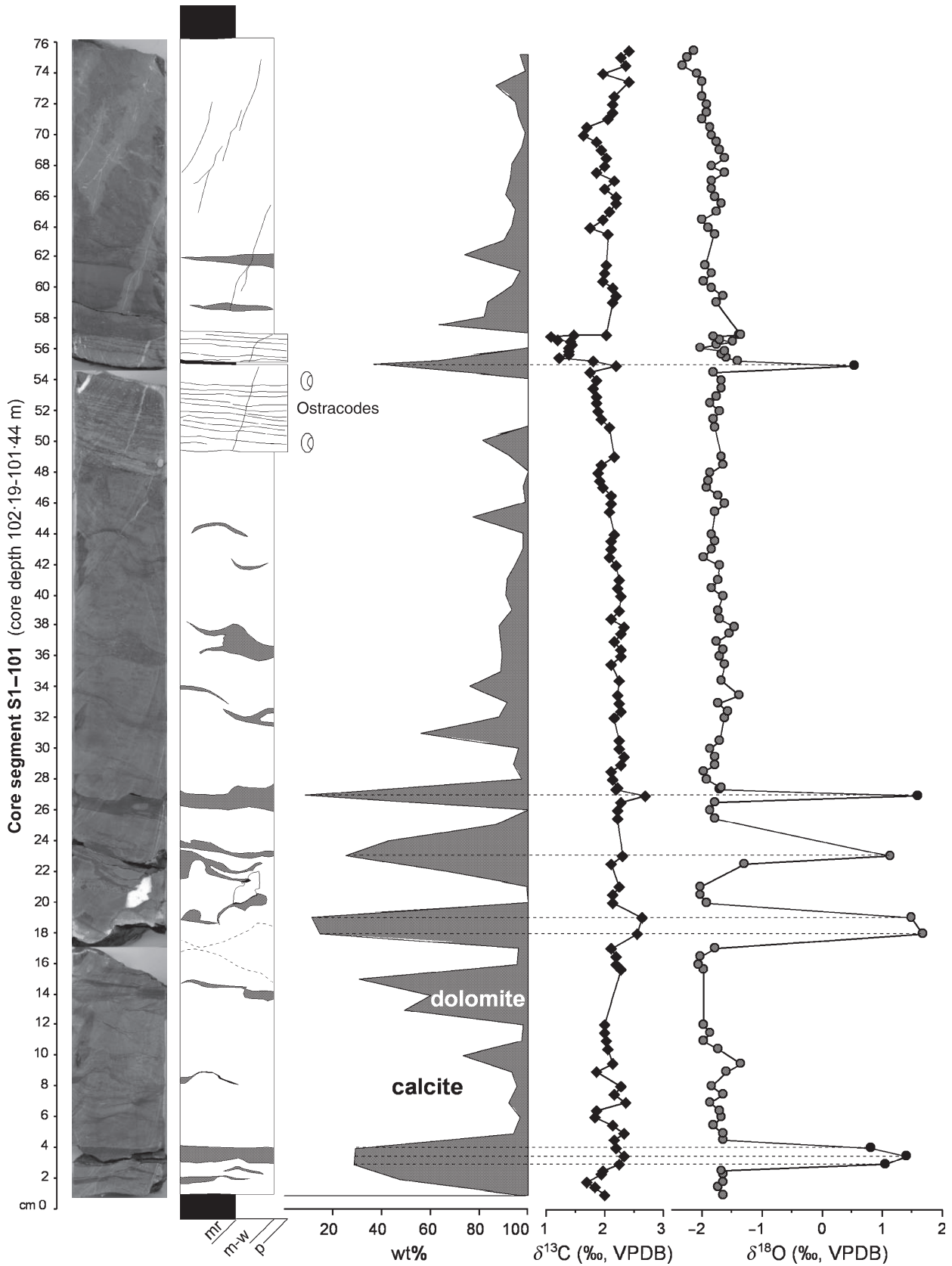


Fig. 9. S1-101 core segment (member A) with calcite-dolomite ratio obtained by Rietveld analysis and stable isotopes values. (mr, mudrock; m, lime mudstone; p, packstone). Calcite-poor dolomite samples are identified by dashed lines (see *Sample material and methods*).

| Sample | a, b (Å) | c (Å) | V (Å ³) | MgCO ₃ (mol%) | | |
|-----------|------------|---------|-----------------------|--------------------------|-----|-----|
| | | | | (1) | (2) | (3) |
| S1-101-03 | 4·9743 | 16·993 | 364·14 | 3·3 | 3·4 | 3·3 |
| S1-101-20 | 4·9749 | 17·017 | 364·75 | 3·2 | 2·3 | 2·8 |
| S1-101-26 | 4·9758 | 17·014 | 364·82 | 3·0 | 2·4 | 2·8 |
| S1-101-51 | 4·9735 | 17·010 | 364·39 | 3·4 | 2·6 | 3·1 |
| S1-101-54 | 4·9718 | 17·004 | 364·00 | 3·8 | 2·9 | 3·4 |
| S1-101-56 | 4·9735 | 17·011 | 364·40 | 3·4 | 2·6 | 3·1 |
| S1-101-57 | 4·9756 | 17·023 | 364·97 | 3·0 | 2·0 | 2·6 |
| Mean | 4·9742 | 17·010 | 364·49 | 3·3 | 2·6 | 3·0 |

MgCO₃ based on regressions of known compositions vs. a parameter (1), c parameter (2), and unit-cell volume (3) following Bischoff *et al.* (1983).

| Sample | a, b (Å) | c (Å) | V (Å ³) | CaCO ₃ (mol%) | | |
|-----------|------------|---------|-----------------------|--------------------------|------|------|
| | | | | (1) | (2) | (3) |
| S1-101-03 | 4·8211 | 16·131 | 324·70 | 54·0 | 56·2 | 54·8 |
| S1-101-18 | 4·8218 | 16·134 | 324·86 | 54·2 | 56·3 | 55·0 |
| S1-101-19 | 4·8225 | 16·136 | 324·99 | 54·4 | 56·4 | 55·1 |
| S1-101-23 | 4·8217 | 16·131 | 324·78 | 54·2 | 56·2 | 54·9 |
| S1-101-27 | 4·8212 | 16·131 | 324·71 | 54·0 | 56·2 | 54·8 |
| S1-101-55 | 4·8242 | 16·148 | 325·46 | 54·9 | 57·0 | 55·6 |
| Mean | 4·8221 | 16·140 | 324·92 | 54·3 | 56·4 | 55·0 |

CaCO₃ based on regressions of NBS calcite standard and dolomite from Lake Arthur vs. a parameter (1), c parameter (2), and unit-cell volume (3) following Reeder & Sheppard (1984).

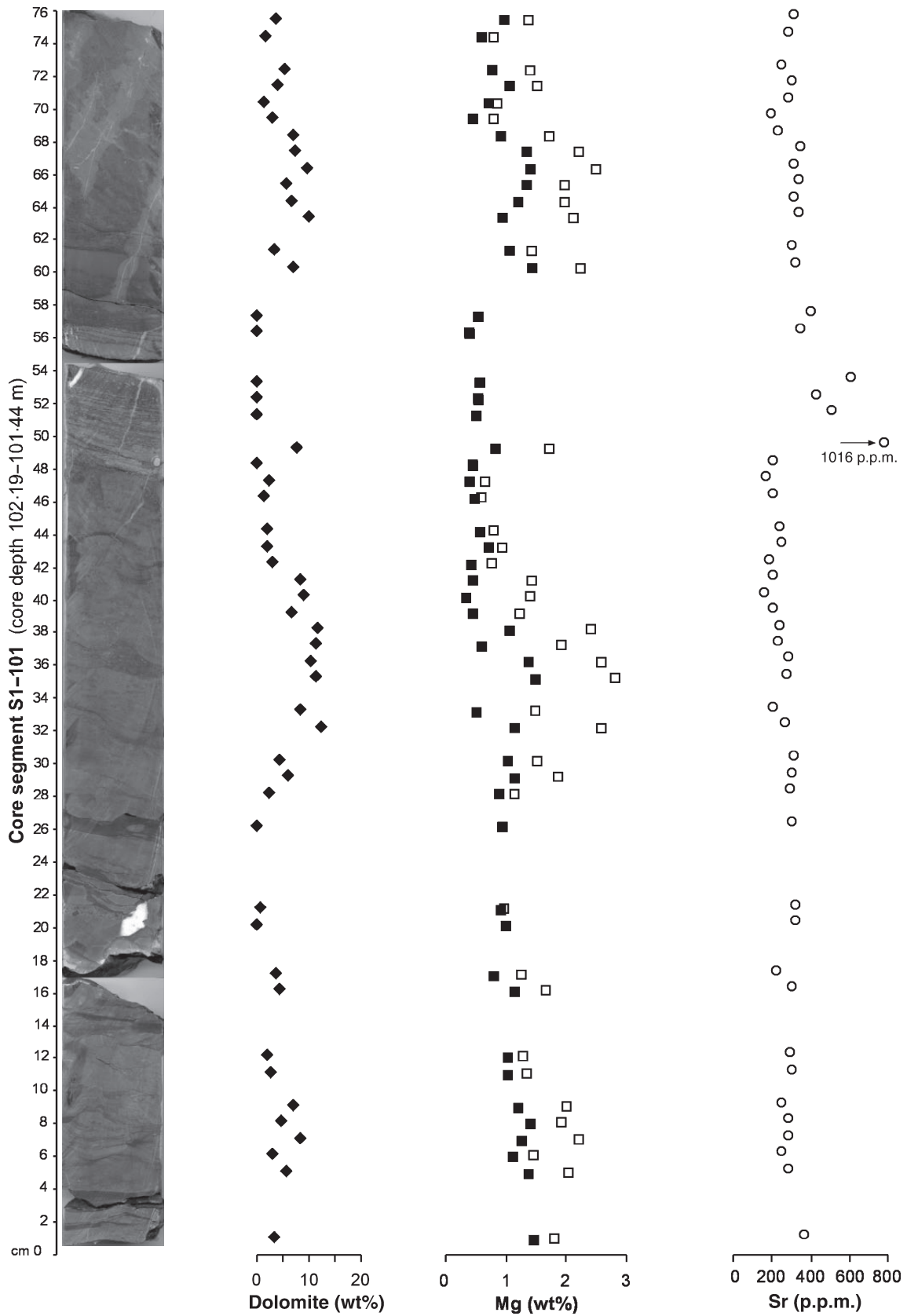
(member A) is essential for the understanding of the environmental change associated with the platform demise. Both sections (Fedares, Lavarella) display an overall thickening and coarsening-upward trend with typical graded calcarenites and breccias as a result of the prograding Lavarella slope. At the top of the more basinward Fedares section, the sediment composition changed as indicated by alternations of breccias, fine-grained turbidites and wavy, non-bioturbated micritic carbonate layers and green mudrocks and marlstones (Figs 4 and 5B). Such layers are absent in stratigraphically deeper positions of the St. Cassian Formation. The absence of bioturbation within these micritic layers (Fig. 5B) and the presence of pyrite suggest the presence of oxygen-depleted basin waters, at least intermittently, at the end of Cassian

Dolomite progradation. This intermittent oxygen-depletion is explained by reduced water circulation because of closure of the Cassian basin by the prograding platforms. The breccia beds at the top of the St. Cassian Formation (Fig. 4) are interpreted as distal, gently dipping slope deposits of the prograding Cassian Dolomite. The colonization of breccia beds by *Thecosmilia* coral colonies (Fig. 4) suggests a prolonged absence of detrital shedding. Similar coral colonies draped by thin-bedded dolomudstones, peloidal to skeletal packstones and micritic crusts were found on top of the arrested, steeply inclined Lavarella palaeoslope (Keim *et al.*, 2001). The limited outcrops of the dolomite bank at Fedares preclude a firm conclusion regarding the palaeorelief, the water depth, and the direction of the slope progradation at this

Table 1. Unit-cell parameters and Mg content of calcite samples of core segment S1-101 (Rietveld analyses).

Table 2. Unit-cell parameters and stoichiometry of dolomite samples of core segment S1-101 (Rietveld analyses).

Fig. 10. S1-101 core segment (member A) with dolomite content obtained by Rietveld analysis and Sr and Mg contents for calcite-rich samples (> 80 wt% calcite). Open squares are Mg values of the bulk samples, whereas the dolomite-corrected compositions are shown by the solid symbols (see text for details).



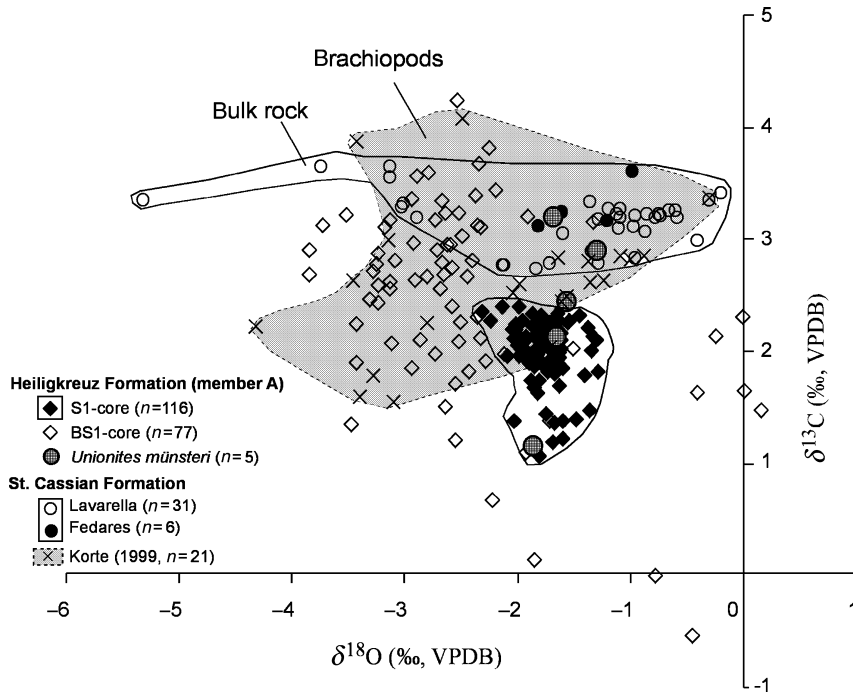


Fig. 11. $\delta^{13}\text{C}$ vs. $\delta^{18}\text{O}$ cross-plot of samples from the uppermost St. Cassian Formation and the basal Heiligkreuz Formation (member A). Not included in this diagram are data for dolomitic limestones from the Fedares and Lavarella sections (see Fig. 4). Brachiopod data from the St. Cassian Formation of Korte (1999) are included for comparison.

Table 3. Rock–Eval and LECO analyses of member A (mudrocks, marlstone and carbonates).

| Samples | Lithology | CaCO ₃ (wt%) | TOC (wt%) | S _{total} (wt%) | C/S | T _{max} (°C) | HI (mg HC/g TOC) |
|------------|--------------|-------------------------|-----------|--------------------------|------|-----------------------|------------------|
| BS1-91 | Mudrock | 16.68 | 0.66 | 0.61 | 1.08 | 416.50 | 31.70 |
| BS1-79.5 | Mudrock | 33.47 | 0.63 | 0.66 | 0.95 | 415.50 | 21.52 |
| BS1-99.5 | Mudrock | 17.21 | 0.87 | 0.61 | 1.43 | 418.50 | 40.39 |
| BS1-49.5 | Marlstone | 75.64 | 0.72 | 0.51 | 1.41 | 423.00 | 377.13 |
| BS1-67.5 | Mudrock | 22.34 | 0.61 | 0.68 | 0.90 | 414.50 | 37.84 |
| BS1-39 | Mudrock | 14.56 | 0.42 | 0.65 | 0.65 | 409.50 | 49.11 |
| BS1-75.8 | Mudrock | 36.36 | 0.62 | 0.81 | 0.77 | 417.00 | 56.39 |
| BS1-85.5 | Mudrock | 21.87 | 0.63 | 0.70 | 0.90 | 425.50 | 34.34 |
| BS1-64 | Mudrock | 13.71 | 0.46 | 0.64 | 0.72 | 421.00 | 28.20 |
| BS1-44 | Mudrock | 35.00 | 0.51 | 0.88 | 0.58 | 415.50 | 35.33 |
| BS1-71 | Mudrock | 29.29 | 0.56 | 0.60 | 0.93 | 415.50 | 60.13 |
| BS1-52 | Mudrock | 25.68 | 0.51 | 1.11 | 0.46 | 410.00 | 28.39 |
| S1-102.16B | Dolomudstone | 94.26 | 0.16 | 0.10 | 1.60 | – | 31.66 |
| S1-101.66A | Dolomudstone | 88.26 | 0.37 | 0.39 | 0.95 | 431.50 | 163.62 |
| S1-102.04F | Dolomudstone | 96.43 | 0.21 | 0.33 | 0.64 | – | 67.63 |
| S1-102.04 | Dolomudstone | 95.09 | 0.20 | 0.13 | 1.54 | – | 58.56 |
| S1-106.05 | Mudrock | 11.81 | 0.21 | 0.06 | 3.50 | – | 0.00 |
| S1-101.40 | Mudrock | 13.11 | 0.38 | 1.36 | 0.28 | – | 21.24 |
| S1-102.48 | Mudrock | 13.24 | 0.23 | 0.63 | 0.37 | – | 4.28 |
| S1-104.17 | Mudrock | 9.80 | 0.34 | 0.59 | 0.58 | 413.50 | 34.01 |
| S1-101.32 | Mudrock | 17.86 | 0.40 | 1.31 | 0.31 | 413.00 | 22.51 |
| S1-100.80 | Mudrock | 28.58 | 0.62 | 1.44 | 0.43 | 419.50 | 27.47 |

location. Extrapolating the geometry of the Lavarella-palaeoslope towards the basin in the north, however, suggests palaeo-water depths in the order of some tens of metres to about 100 m (Fig. 2C).

The contact between the topmost Cassian Dolomite and the basal Heiligkreuz Formation (member A) was not penetrated in the bore holes, but is exposed in one small outcrop near Fedares. There the light-coloured Cassian Dolomite is

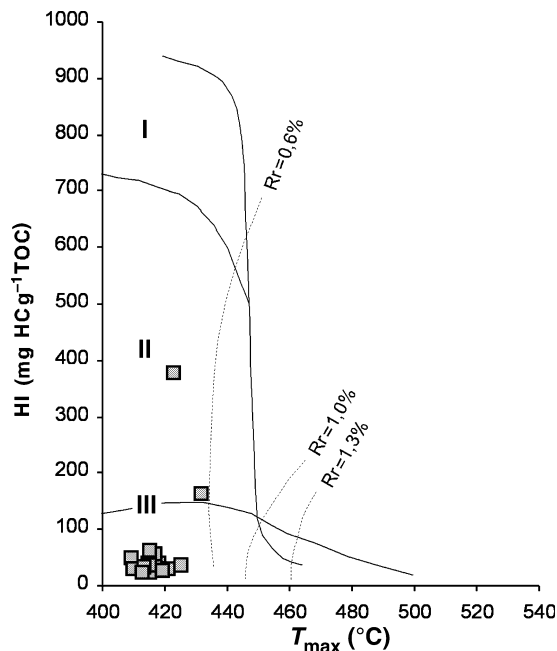


Fig. 12. Hydrogen index (HI) vs. T_{\max} plot (kerogen types) of samples from member A. The prevailing kerogen type III indicates a terrestrial origin of the organic matter. HI = ratio between S2 [= residual petroleum potential that has not yet been used to generate hydrocarbons] and TOC (mg HC/g TOC)]. T_{\max} ($^{\circ}\text{C}$) = temperature at which the maximum amount of hydrocarbons is generated.

capped by bituminous lime mudstones devoid of platform-derived grains. Observations on the Lavarella palaeoslope are consistent with such a sharp lithological change. Ostracod-rich, black marlstones and skeletal packstones (member A) cover the arrested, steep Lavarella carbonate slope (Figs 1 and 2C). Black marlstones, however, are absent on the platform top indicating that it remained sub-aerially exposed during deposition of member A in the intervening basin (or that such deposits were later eroded).

The most striking difference between member A and the St. Cassian Formation, therefore, is the absence of any evidence of platform or slope shedding in member A lithologies as well as the absence of a diverse fauna as described from the underlying St. Cassian Formation (e.g. Fürsich & Wendt, 1977; Wendt & Fürsich, 1980; Urlichs, 1994; Broglio Loriga *et al.*, 1999). Most of the carbonate of member A (skeletal and non-skeletal grains, peloidal limestones) is interpreted as autochthonous formation within the HHB. The presence of clotted and microcolumnar fabrics and micritic crusts (Fig. 7C–F) within the peloidal limestones is indicative of *in situ* carbonate

precipitation, probably under the presence of microbial or organic mats (e.g. Monty, 1995; Riding, 2000). The carbonate precipitation in the HHB was frequently interrupted by the high influx of smectitic clays and terrestrial organic matter. The presence of blackened lithoclasts and blackened ostracod shells within member A suggests proximal vegetated land as blackening of fossils and lithoclasts commonly results from interaction with reactive terrestrial organic matter in the shallow-marine or sub-aerial environment (e.g. Strasser & Davaud, 1983).

The organic matter, which reaches up to 0.9 wt%, was derived largely from land plants as indicated by the low hydrogen index (Fig. 12). This is consistent with the setting of the HHB between platforms, which most likely formed islands during deposition of member A. Two samples, however, suggest kerogen type II, i.e. marine algae and bacteria, which is consistent with the fabrics attributed to microbial mats in the carbonates of member A. The high influx of nutrients (terrestrial organic matter and weathering products) during sedimentation of member A would have led to enhanced bioproductivity and possibly episodic eutrophication, e.g. in the form of putative microbial mats (Fig. 7C–E) and abundant assemblages of low-diversity ostracods (see below). High nutrient load in conjunction with sluggish water circulation within this restricted basin resulted in the episodic reduction of oxygen in the bottom water as indicated by the widespread presence of framboidal pyrite (a product of bacterial sulphate reduction, e.g. Oschmann, 2000), alternating bioturbated and non-bioturbated layers, and the general low diversity of bottom-dwelling fauna. The low C_{org}/S ratios (mean 0.96) support marine conditions.

In summary, the Lower Carnian platform demise induced a distinct switch in the locus of carbonate production from the former platform and slope to the HHB. Filling of the HHB by the end of member A deposition produced a shallow-water basin as testified by the presence of fenestral dolomite on top of member B. Thereafter, mixed carbonate-coarse siliciclastics (member C) covered the HHB and the platform top (Fig. 2C).

From open-marine to basin restriction: the biological response

Ostracods

The ostracod fauna of member A is dominated by abundant occurrences of the species *R. santacrucis* and *S. brotzenorum nostorica* suggesting a

stressed and possibly oxygen-depleted environment. The close association of ostracods and peloidal packstones and micritic crusts (Fig. 7C and D) suggests that these carbonate layers served as substrate for the ostracod fauna. *R. santacrucis* as well as *Reubenella* sp. are regarded as a typical marine fauna (Kristan-Tollmann & Hamedani, 1973; Gerry *et al.*, 1990), whereas *S. brotzenorum* is known from both brackish and hypersaline environments (Gerry *et al.*, 1990). Based on the occurrence of normal-marine and brackish-water ostracod assemblages in the Carnian succession of Israel, Gerry *et al.* (1990) postulated an oscillating salinity trend induced by sea-level fluctuations. Feldman *et al.* (2001) attributed the combined occurrences of *S. brotzenorum* and the marine ostracod genera (*Reubenella*, *Leviella* and *Mockella*) within the Saharonim Formation (Carnian; Israel) to mixing of marine and continental waters. In the present study of the Heiligkreuz Formation, the co-occurrence of typical marine genera and the euryhaline genus *Simeonella* within the same strata suggest that both fauna lived together in normal marine water.

A further particularity of member A are bivalve coquinas (*Unionites münsteri*) preferentially within mudrocks and marlstones (Figs 6 and 7A). These coquinas cannot be attributed to storm events because they lack sedimentary structures (e.g. hummocky cross-stratification, graded beds). Unfortunately, little is known about the palaeoecology of this genus. C and O isotope data (see above) from the aragonitic *Unionites* shells suggest normal marine water (Fig. 11) given that their compositions overlap those of typical fresh- or brackish-water bivalves ($\delta^{13}\text{C}$ values of $\leq -5\text{‰}$ and rather negative $\delta^{18}\text{O}$ values, Yin *et al.*, 1995). Thus *Unionites münsteri* is considered a normal marine taxum. Monospecific mass occurrences of bivalves are typical of stressed, oxygen-depleted environments and are commonly explained by *in situ* mass mortality as a result of a rising $\text{O}_2/\text{H}_2\text{S}$ interface (e.g. Oschmann, 1991; Sageman *et al.*, 1991; Röhl *et al.*, 2001). Thus, *Unionites* coquinas are interpreted as mass-mortality assemblages at times when anoxia extended intermittently above the sediment-water interface.

The biological evidence provides no evidence of hypersaline or brackish water conditions during deposition of member A. Mass occurrences of ostracods and bivalves, however, imply an ecologically stressed environment. Given the widespread presence of pyrite it is speculated that oxygen depletion and/or terrestrially derived

high nutrient load were the stress factors in this environment.

From open-marine to basin restriction: geochemical proxies

Are primary depositional signals preserved?

Trace elements and stable isotopes in carbonate minerals can provide useful constraints on the composition of the original fluid from which they precipitated provided that these minerals have not been altered subsequently. This assumption is generally violated as the majority of marine carbonates undergo some sort of early diagenesis giving rise to a thermodynamically stable mineralogical and chemical composition. Carbonates sandwiched between impermeable shales, however, are less prone to diagenetic alteration (Pearson *et al.*, 2001). In fact one of the classic studies demonstrating this convincingly is the one by Scherer (1977) on aragonitic macrofossils which are preserved because they were sealed within mudrocks of the St. Cassian Formation. Rocks of member A show even a higher mudrock-to-carbonate ratio which provides excellent conditions for the preservation of near-pristine compositions. The low diagenetic overprint of the St. Cassian Formation and member A is shown by (a) the presence of aragonite shells (*Unionites münsteri*) and traces of high-Mg calcite, (b) the abundance of non-stoichiometric dolomite, (c) the complete absence of coarsely crystalline (recrystallized) carbonates and (d) the abundance of smectite in the intervening mudrocks. There is, however, petrographic evidence of early diagenesis in member A, as shown by chemical (and locally also mechanical) compaction features and moderately bright CL of carbonate cements. A conspicuous feature of carbonates of member A is the common presence of finely crystalline, non-stoichiometric (Ca-rich) dolomite typical of early diagenetic precipitation (e.g. Searl, 1994; Lumsden & Lloyd, 1997). The close association of dolomite, pyrite and organic matter (Figs 7B and 8B) suggests a possible link between sulphate reduction and the precipitation of dolomite (organogenic dolomites, Baker & Kastner, 1981; Wright, 1999; Burns *et al.*, 2000). The low Fe content and the weak CL colour is consistent with this interpretation. Dolomite appears to have formed prior to and possibly also during pressure solution (Fig. 7B) that is known to commence under very shallow burial conditions in carbonate sediments (Shinn & Robbin, 1983). As zones of intense pressure solution (solution seams) are

almost invariably associated with higher amounts of organic matter (and other insoluble residue), the precipitation of dolomite may not be directly linked to compaction (Wanless, 1979) but rather to the presence of organic matter undergoing sulphate reduction.

In essence, the minimal diagenesis of these mudrock-dominated sediments suggests that geochemical data of the present-day rocks can be used as fairly reliable proxies of the initial environmental conditions.

Results of the present study are based on bulk samples only (with the exceptions of *Unionites* shells) and, therefore, represent mixtures. The discussion is limited to dolomite-poor carbonate samples, but it is acknowledged that these samples underwent burial diagenesis, albeit in a semi-closed system sealed by mudrocks. Sr concentrations of the St Cassian Formation at Fedares and Lavarella (99–1026 p.p.m.; mean of 495 ± 203) are lower than those of low-Mg brachiopods from the St. Cassian Formation at Stuoress Wiesen/Prati di Stuoress, located some 5 km south of Lavarella (350–1941 p.p.m., mean of $921 (\pm 452)$ p.p.m. – Steuber & Veizer, 2002) and also generally lower than those of modern marine calcites (including biota and cements – e.g. Milliman, 1974), thus suggesting some mineral stabilization during burial. High-resolution sampling of core segment S1-101 reveals rather stable Sr values of *c.* 180–400 p.p.m. except for a few scattered higher values associated with a thin layer of ostracod packstone (Fig. 10). These values are within the range obtained from the underlying St. Cassian Formation (Fig. 4). Given the fact that the St. Cassian Formation are fully marine pelagic deposits, similar Sr values in member A argue against a significant long-term change in the Sr concentration of the sea water before and after the platform demise.

Magnesium values are more difficult to interpret because of the presence of variable proportions of dolomite in member A. When corrected for the presence of dolomite, calcite-rich samples show Mg contents between 0.35 and 1.5 wt%. Low Mg-calcite that precipitated inorganically from modern sea water is expected to have a theoretical Mg content of ≥ 1.6 wt%, the exact number depending among others on the mole per cent Mg in the calcite (see Morse & Bender, 1990 and Mucci & Morse, 1990). As the Mg/Ca ratio of Triassic sea water was probably close to modern sea water (Hardie, 1996; Lowenstein *et al.*, 2001), the Mg values measured in calcites of member A (0.35–1.5 wt%) imply lower Mg/Ca ratios in the

water of the HHB. More likely, however, these low Mg contents are the result of early diagenetic stabilization (Choquette & James, 1990; Andrews, 1991). It is noted that Scherer (1977: fig. 16) reported Mg values in carbonates of the St. Cassian Formation (0.6–2 wt% Mg) which are also somewhat lower than expected marine values and which he attributed to diagenesis of biocalcarenes. In essence, the Mg values along with Sr contents of calcitic samples from member A are consistent with a near-normal marine sea water origin. It is suggested that Mg released during stabilization processes favoured subsequent precipitation of early diagenetic dolomite.

Bulk-rock stable C and O isotope values of the upper St. Cassian Formation are consistent with published values from other sections in the region (Scherer, 1977; Korte, 1999; Veizer *et al.*, 1999), and largely overlap the isotopic values of carbonate beds within member A (Fig. 11). This array of stable C and O values is similar to the one defined by well-preserved brachiopods (Korte, 1999; Veizer *et al.*, 1999). In addition, aragonite-rich *Unionites* shells also plot within this field (Fig. 11). Taken together, the data suggest low levels of diagenetic overprinting and rather similar C and O isotopic compositions between member A and its fully marine precursor (St. Cassian Formation).

When compared with the data set of Veizer *et al.* (1999), present data from both the St. Cassian Formation and member A fall on the Triassic portion of the Phanerozoic isotope trends (C and O). Late Julian stable isotope data may contribute toward refining the structure of the long-term isotope curve.

A shift toward lower $\delta^{13}\text{C}$ values in some samples from the BS1 core and throughout core segment S1-101 (Fig. 9) may be attributed to the incorporation of ^{13}C -depleted carbon released during bacterial sulphate reduction (consistent with the presence of pyrite). High-resolution stable-isotope sampling within core segment S1-101 shows no evidence of significant high-frequency changes except for a small, short-lived excursion toward lower $\delta^{13}\text{C}$ values at 55–58 cm in the core (Fig. 9). Major changes in both C and O isotope values are otherwise always associated with the presence of dolomite (Fig. 9).

Palaeoceanographic consequences in the aftermath of the platform demise

The Cassian platforms in the Dolomites were characterized by strong lateral growth during the Early Carnian that led to a closure of most of the

intervening basins and to a levelling out of the former platform-to-basin relief. In the topmost basinal sediments at Fedares, thin, non-bioturbated carbonate layers indicate interruptions of platform and slope shedding and a shift of the Late Cassian basin towards an intermittent oxygen-depleted environment (Fig. 13). The depletion of oxygen in the Late Cassian basin can be explained by restricted circulation caused by the closure of the basins by the prograding platforms. At Lavarella the abandoned steep (*c.* 20°) palaeoslope was successively colonized by a few small coral mounds and subsequently draped by skeletal packstones and microbial bindstones (Keim *et al.*, 2001). Judging from the height of the Lavarella palaeoslope, the depth of the HHB following the platform demise was about 100 m (Fig. 2C).

The earliest rocks at Fedares and Lavarella immediately covering the abandoned carbonate slopes and mounds – mudrocks, marls and bituminous mudstones – indicate a fundamental change in the hydrography of the region. What exactly caused the demise of the Carnian platforms remains an unresolved issue. One hypothesis relates the termination of the growth of the Cassian Dolomite platforms to a relative sea-level drop with consequent sub-aerial exposure and karstification (Bosellini, 1984; De Zanche *et al.*, 1993). Other limiting factors for platform growth such as termination of regional subsidence, increased levels of nutrients, oxygen-depletion and salinity fluctuations have also been previously invoked (Keim *et al.*, 2001). Finally, a change from arid to intermittently humid conditions and a concomitant increase in terrestrially derived nutrients may have occurred at the Julian–Tuvalian boundary (e.g. Simms & Ruffell, 1989; Simms *et al.*, 1995; Gianolla *et al.*, 1998b; Berra & Jadoul, 2002; Preto & Hinnov, 2003; Stefani *et al.*, 2004).

According to Simms & Ruffell (1989) and Simms *et al.* (1995) this climate change was responsible for various palaeoecological crises and mass extinctions in the marine and terrestrial realm during the Late Julian and Tuvalian. With the present data we can neither confirm nor exclude a climate change as a major cause for the platform demise in the study area. In the Dolomites region, the occurrences of amber (Gianolla *et al.*, 1998b) and the character of palaeosol horizons (Preto & Hinnov, 2003; Stefani *et al.*, 2004) in the lower and middle parts of the Heiligkreuz Formation have been interpreted as indicators of more humid conditions. Ammonoids indicate a Late Julian to Early Tuvalian age for this inferred palaeoclimate change (Gianolla *et al.*, 1998b; De Zanche *et al.*, 2000). These climate-sensitive records, however, occur stratigraphically > 60 m above the boundary marking the demise of the Cassian platform (Preto & Hinnov, 2003; Stefani *et al.*, 2004), and thus this shift to wetter conditions may have occurred after platform demise. Indeed, the high influx of terrestrial organic matter and smectitic clays post-dating the platform demise, as recorded within member A (Fig. 13), indicates enhanced weathering and runoff. A climatic change to intermittent humid conditions at the Julian/Tuvalian boundary was further indicated on the basis of pollen and spores from the Conzen and Tor Formations in the Julian Alps of NE Italy (Roghi, 2004).

The absence of rocks of member A on the platforms is in agreement with the postulated sea-level drop at the end of the Cassian Dolomite (Fig. 13). A sea-level drop in the order of only a few metres would have been sufficient to expose large platform areas given that most of the initial platform-to-basin palaeotopography was minimized by the Late Julian. The occurrence of member A in the HHB is considered as a sea-level lowstand deposit and is consistent with the proposed

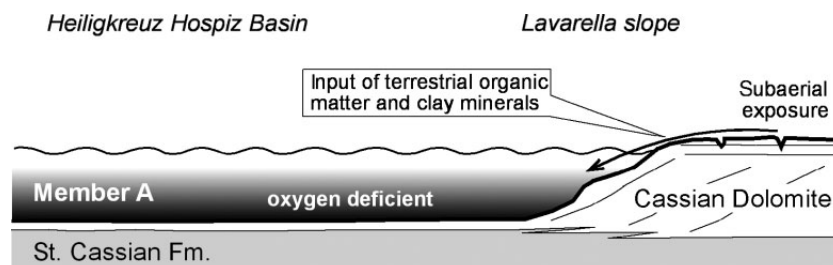


Fig. 13. Depositional model for the region following the demise of the shallow-water carbonate platforms. Oxygen-deficient waters post-dating the platform demise extended at least temporarily to the uppermost Lavarella slope, as indicated by the superposition of dark marlstones of member A on normal-marine mounds on top of the Cassian Dolomite.

shelf margin wedge of the Car 3 depositional sequence in the Dolomites (De Zanche *et al.*, 1993). This model is also in concordance with that of Nagy (1999) who also postulated a sea-level drop and basin restriction for the formation of Carnian bituminous laminites in the lower part of the Sándorhegy Formation (Pécsely Mb.) in the Balaton Highland (Hungary).

As a consequence of the inferred sea-level drop, circulation in the semi-closed HHB may have become sluggish giving rise to low oxygen levels in its bottom waters as the influx of organic matter in member A exceeded the oxidation capacity of the bottom water (Fig. 13). As a result, the HHB may have turned into an intermittently dysaerobic, stressed environment with repeated occurrences of low-diversity biota. The presence of early diagenetic dolomite is consistent with oxygen-depleted, reducing conditions in the topmost sediments of this basin. In the present case study, it is inferred that dysaerobic conditions extended at least temporarily up to the uppermost Lavarella slope, while the platform top was probably sub-aerially exposed (Fig. 13).

The occurrence of organic-rich mudstones in the HHB is not a local phenomenon. Contemporaneous black shales facies of Late Julian to Early Tuvallian age have been documented from various places in the western Tethys Ocean, e.g. in the Northern Calcareous Alps (Reingrabenschiefs, *Halobia* schists: Schlager & Schöllnberger, 1974; Gawlick & Lein, 1997; Hornung & Brandner, 2005), the Balaton Highland of Hungary (Pécsely Mb. of the Sándorhegy Formation: Nagy, 1999) and in the Sicani Mountains of Sicily ('*Halobia*-bearing cherty calcilitites': Bellanca *et al.*, 1995). It is interesting to note that even the deep-marine Tethys Ocean – the Hallstatt basin of the Northern Calcareous Alps – was affected by a major change in the sedimentation style at this time suggesting that the change in sedimentation style and geochemical changes observed in the study area record a palaeoceanographic event of widespread extent.

CONCLUSIONS

Member A of the Heiligkreuz Formation represents a hitherto poorly known succession of basinal deposits that record a major change in the Carnian platform evolution of the Dolomites. This study relies on newly available material from drill cores supplemented by outcrop data from the underlying fully marine St. Cassian Formation.

The key observation is the abrupt shutdown of shallow-water carbonate production manifested by a switch from calciturbidite layers of the St. Cassian Formation to micritic and peloidal carbonates that filled the remaining HHB as well as enhanced influx of terrestrially derived organic matter. Carbonate precipitation in the HHB is interpreted as being to some extent controlled by microbial communities. Geochemical data suggest no fundamental changes in sea water composition of the basin across the transition to the post-platform succession. Petrographic and geochemical data indicate a decrease in the availability of dissolved oxygen in bottom waters synchronously with the change in sedimentation style. Comparison with other field regions suggest that the change in sedimentation style recorded in the HHB was probably the manifestation of a palaeoceanographic event that affected large areas of the northwestern Tethys Ocean.

ACKNOWLEDGEMENTS

This study was made possible by the Kreuzkofel drilling project initiated by the Geological Survey of Bozen/Bolzano. We greatly thank L. Nössing for providing technical and financial support. Special thanks go to the excellent drilling team of L. Planer and W. Pignater. The director of the Natural Park Fanes-Sennes-Prags, A. Kammerer, granted access to the drill location. We gratefully acknowledge L. Krystyn (Vienna) for conodont analysis, W. Mette (Innsbruck) for determination of the ostracod fauna, T. Rainer and R. F. Sachsenhofer (Leoben) for pyrolysis analyses, M. Wimmer (Innsbruck) for assistance in the stable-isotope laboratory and A. Saxer (Innsbruck) for help with the SEM. M. Urlichs (Stuttgart) and G. Geyer (Würzburg) kindly shared valuable information about the fossil contents of the Heiligkreuz Formation. Detailed comments by P. Enos, P. Gianolla and an anonymous referee, as well as Co-editor I. Montañez are highly appreciated.

This study was partially supported by the Austrian Fonds zur Förderung der wissenschaftlichen Forschung (FWF-Project P11918-TEC, R. Brandner) and by the Geological Survey of the Autonomous Province of Bozen/Bolzano.

REFERENCES

- Andrews, J.E. (1991) Geochemical indicators of depositional and early diagenetic facies in Holocene carbonate muds,

- and their preservation potential during stabilisation. *Chem. Geol.*, **93**, 267–289.
- Assereto, R., Brusca, C., Gaetani, M. and Jadoul, F.** (1977) The Pn–Zn mineralization in the Triassic of the Dolomites – geological history and genetic interpretations. *Industria Miner.*, **28**, 267–302.
- Baker, P. and Kastner, M.** (1981) Constraints on the formation of sedimentary dolomite. *Science*, **213**, 214–216.
- Bathurst, R.G.C.** (1987) Diagenetically enhanced bedding in argillaceous platform limestones: stratified cementation and selective compaction. *Sedimentology*, **34**, 749–778.
- Bellanca, A., Di Stefano, P. and Neri, R.** (1995) Sedimentology and isotope geochemistry of Carnian deep-water marl/limestone deposits from the Sicani Mountains, Sicily: environmental implications and evidence for a planctonic source of lime mud. *Palaeogeogr. Palaeoclim. Palaeoecol.*, **114**, 111–129.
- Berner, R.A. and Raiswell, R.** (1984) C/S method for distinguishing freshwater from marine sedimentary rocks. *Geology*, **12**, 365–368.
- Berra, F. and Jadoul, F.** (2002) Evidence of a “mid-Carnian” transgression in the western Southern Alps (Lombardy, Italy): stratigraphic and paleogeographic implications. *Riv. Ital. Paleontol. Stratigr.*, **108**, 119–131.
- Biddle, K., Schlager, W., Rudolph, K.W. and Bush, T.** (1992) Seismic model of a progradational carbonate platform, Picco di Vallandro, the Dolomites, Northern Italy. *Am. Assoc. Petrol. Geol. Bull.*, **76**, 14–30.
- Bischoff, W.D., Bishop, F.C. and Mackenzie, F.T.** (1983) Biogenically produced magnesian calcite: inhomogeneities in chemical and physical properties; comparison with synthetic phases. *Am. Mineral.*, **68**, 1183–1188.
- Bish, D.L. and Post, D.E.** (1993) Quantitative mineralogical analysis using the Rietveld full-pattern fitting method. *Am. Mineral.*, **78**, 932–940.
- Bizzarini, F. and Rottonara, E.** (1997) La tanatocenosi a vertebrati delle Heiligenkreuzschichten in Alta Val Badia, Dolomiti. *Boll. Mus. civ. nat. Venezia*, **47**, 307–316.
- Bosellini, A.** (1984) Progradation geometries of carbonate platforms: examples from the Triassic of the Dolomites, Northern Italy. *Sedimentology*, **31**, 1–24.
- Bosellini, A. and Largaiolli, T.** (1965) Contributo alla conoscenza degli strati di S. Croce (Val Badia – Dolomiti). *Studi Trent. Sci. Nat., Sez. A*, **42**, 5–12.
- Bosellini, A., Masetti, D. and Neri, C.** (1982) La geologia del Passo del Falzarego. In: *Guida alla Geologia del Sudalpino Centro-Orientale* (Eds A. Castellarin and G.B. Vai), pp. 273–278, Soc. Geol. It., Guide Geol. Reg., Bologna.
- Bosellini, A., Neri, C. and Stefani, M.** (1996) *Geologia delle Dolomiti. Introduzione Geologica*. Guida alla Escursione Generale, 78a Riunione Estiva della Soc. Geol. It., S. Cassiano (Italy), 120 pp.
- Brandner, R.** (1984) Meeresspiegelschwankungen und Tektonik in der Trias der NW-Tethys. *Jb. Geol. B.-A.*, **126**, 435–475.
- Broglio Loriga, C., Cirilli, S., De Zanche, V., Di Bari, D., Gianolla, P., Laghi, G.F., Lowrie, W., Manfrin, S., Mastradrea, A., Mietto, P., Muttoni, G., Neri, C., Posenato, R., Reichichi, M., Rettori, R. and Roghi, G.** (1999) The Prati di Stuares/Stuares Wiesen Section (Dolomites Italy): a candidate Global Stratotype Section and Point for the base of the Carnian stage. *Riv. Ital. Paleontol. Stratigr.*, **105**, 37–78.
- Burns, S.J., McKenzie, J.A. and Vasconcelos, C.** (2000) Dolomite formation and biogeochemical cycles in the Phanerozoic. *Sedimentology*, **47**(Suppl. 1), 49–61.
- Castellarin, A., Lucchini, F.A., Rossi, P.L., Selli, L. and Simboli, G.** (1988) The Middle Triassic magmatic–tectonic arc development in the Southern Alps. *Tectonophysics*, **146**, 79–89.
- Choquette, P.W. and James, N.P.** (1990) Limestones – the burial diagenetic environment. In: *Diagenesis* (Eds I.A. McIlreath and D.W. Morrow), *Geosci. Can. Reprint Ser. (Geol. Assoc. Can.)*, **4**, 75–111.
- Dalla Vecchia, F.M. and Avanzini, M.** (2002) New findings of isolated remains of Triassic reptiles from Northeastern Italy. *Boll. Soc. Paleontol. It.*, **41**, 215–235.
- De Zanche, V., Gianolla, P., Mietto, P., Siorpaes, C. and Vail, P.** (1993) Triassic sequence stratigraphy in the Dolomites. *Mem. Sci. Geol.*, **45**, 1–27.
- De Zanche, Gianolla, P. and Roghi, G.** (2000) Carnian stratigraphy in the Raibl/Cave del Predil area (Julian Alps, Italy). *Eclogae. Geol. Helv.*, **93**, 331–347.
- Feldman, H.R., Rosenfeld, A., Samp, S. and Greenfield, R.** (2001) Paleocology and biogeography of the Sephardic Province prior to the Carnian (Triassic) salinity crisis. In: *36th Geol. Soc. Am. Annual Meeting*, March 12–14, 2001, Northeastern Section, Burlington, Vermont.
- Fürsich, F.T. and Wendt, J.** (1977) Biostratigraphy and palaeoecology of the Cassian Formation (Triassic) of the Southern Alps. *Palaeogeogr. Palaeoclim. Palaeoecol.*, **22**, 257–323.
- Gawlick, H.-J. and Lein, R.** (1997) Neue stratigraphische und fazielle Daten aus dem Jakobberg – und Wolfdietrichstollen des Hallein – Bad Dürrenberger Salzberges und ihre Bedeutung für die Interpretation der geologischen Verhältnisse im Bereich der Hallein – Berchtesgadener Schollenregion. *Geol. Paläont. Mitt. Innsbruck*, **22**, 199–225.
- Gerry, E., Honigstein, A., Rosenfeld, A., Hirsch, F. and Eshet, Y.** (1990) The Carnian salinity crisis: ostracods and palynomorphs as indicators of palaeoenvironment. In: *Ostracoda and Global Events* (Eds R. Whatley and C. Maybury), pp. 87–99. Chapman & Hall, London.
- Gianolla, P., De Zanche, V. and Mietto, P.** (1998a) Triassic sequence stratigraphy in the Southern Alps (Northern Italy). Definition of sequences and basin evolution. In: *Mesozoic–Cenozoic Sequence Stratigraphy of European Basins* (Eds P.C. De Graciansky, J. Hardenbol, T. Jacquin and P.R. Vail). *SEPM Spec. Publ.*, **60**, 723–751.
- Gianolla, P., Ragazzi, E. and Roghi, G.** (1998b) Upper Triassic amber from the Dolomites (Northern Italy). A paleoclimatic indicator? *Riv. Ital. Paleontol. Stratigr.*, **104**, 381–390.
- Hardie, L.A.** (1996) Secular variation in seawater chemistry: an explanation for the coupled secular variation in the mineralogies of marine limestones and potash evaporites over the past 600 m.y. *Geology*, **24**, 279–283.
- Hochuli, P.A. and Frank, S.M.** (2000) Palynology (dinoflagellate cysts, spore-pollen) and stratigraphy of the Lower Carnian Raibl Group in the Eastern Swiss Alps. *Eclogae geol. Helv.*, **93**, 429–443.
- Hornung, T. and Brandner, R.** (2005) Biochronostratigraphy of the Reingraben Turnover (Hallstatt Facies Belt): local black shale events controlled by regional tectonics, climatic change and plate tectonics. *Facies*, **51**, 460–479.
- Keim, L., Brandner, R., Krystyn, L. and Mette, W.** (2001) Termination of carbonate slope progradation: an example from the Carnian of the Dolomites, Northern Italy. *Sediment. Geol.*, **143**, 303–323.
- Koken, E.** (1913) Beiträge zur Kenntnis der Schichten von Heiligenkreuz (Abteital, Südtirol). *Abh. Geol. Reichsanst. Wien*, **16/4**, 56 pp.

- Korte, C.** (1999) $^{87}\text{Sr}/^{86}\text{Sr}$, $\delta^{18}\text{O}$ - und $\delta^{13}\text{C}$ -Evolution des triassischen Meerwassers: Geochemische und stratigraphische Untersuchungen an Conodonten und Brachiopoden. *Bochumer geol. u. geotechn. Arb.*, **52**, 1–171.
- Kristan-Tollmann, E. and Hamedani, A.** (1973) Eine spezifische Mikrofaunen-Vergesellschaftung aus den Opponitzer Schichten des Oberkarn der nieder-österreichischen Kalkvorlpen. *N. Jb. Geol. Paläont. Abh.*, **143**, 193–222.
- Krystyn, L.** (1979) Eine neue Zonengliederung im alpin-mediterranen Unterkarn. In: *Beiträge zur Biostratigraphie der Tethys-Trias* (Ed. H. Zapfe). *Österreichische Akademie der Wissenschaften, Erdwissenschaftliche Schriftenreihe*, **4**, 37–75.
- Krystyn, L.** (1998) Der Lunz-Event: die größte Ökosystemkrise der marinen Trias. *5. Jahrestagung Österr. Paläontolog. Ges.*, 1 p.
- Leonardi, P.** (1967) *Le Dolomiti. Geologia dei monti tra Isarco e Piave*. 2 Vol, Edizioni Manfrini, Rovereto, 1019 pp.
- Liebermann, H.M.** (1979) Die Bivalven- und Ostracodenfauna von Raibl und ihr stratigraphischer Wert. *Verh. Geol. B-A*, **1979**, 85–131.
- Lowenstein, T.K., Timofeeff, M.N., Brennan, S.T., Hardie, L.A. and Demicco, R.V.** (2001) Oscillations in phanerozoic seawater chemistry: evidence from fluid inclusions. *Science*, **294**, 1086–1099.
- Lumsden, D.N. and Lloyd, R.V.** (1997) Three dolomites. *J. Sed. Res.*, **67**, 391–396.
- Masetti, D., Neri, C. and Bosellini, A.** (1991) Deep-water asymmetric cycles and progradation of carbonate platforms governed by high frequency eustatic oscillations (Triassic of the Dolomites, Italy). *Geology*, **19**, 336–339.
- Milliman, J.D.** (1974) *Marine Carbonates*. Springer-Verlag, New York, 375 pp.
- von Mojsisovics, E.M.** (1879) *Die Dolomit-Riffe von Südtirol und Venetien: Beiträge zur Bildungsgeschichte der Alpen*. A. Hölder, Wien. 551 pp.
- Monty, C.L.V.** (1995) The rise and nature of carbonate mudmounds: an introductory actualistic approach. In: *Carbonate Mud-Mounds. Their Origin and Evolution* (Eds C.L.V. Monty, D.W.J. Bosence, P.H. Bridges and B.R. Pratt). *Spec. Publ. Int. Assoc. Sediment.*, **23**, 11–48.
- Morse, J.W. and Bender, M.L.** (1990) Partition coefficients in calcite: examination of factors influencing the validity of experimental results and their application to natural systems. *Chem. Geol.*, **82**, 265–277.
- Mucci, A. and Morse, J.W.** (1990) Chemistry of low-temperature abiogenic calcites: experimental studies on coprecipitation, stability, and fractionation. *Aquat. Sci.*, **3**, 217–254.
- Nagy, Z.R.** (1999) Platform-basin transition and depositional models for the Upper Triassic (Carnian) Sándorhegy Limestone, Balaton Highland, Hungary. *Acta Geol. Hung.*, **42/3**, 267–299.
- Oschmann, W.** (1991) Distribution, dynamics and palaeoecology of Kimmeridgian (Upper Jurassic) shelf anoxia in western Europe. In: *Modern and Ancient Continental Shelf Anoxia* (Eds R.V. Tyson and T.H. Pearson). *Geol. Soc. London Spec. Publ.*, **58**, 381–395.
- Oschmann, W.** (2000) Microbes and black shales. In: *Microbial Sediments* (Eds R.E. Riding and S.M. Awramik), pp. 137–148. Springer, Berlin.
- Pearson, P.N., Ditchfield, P.W., Singano, J., Harcourt-Brown, K.G., Nicholas, C.J., Olsson, R.K., Shackleton, N.J. and Hall, M.A.** (2001) Warm tropical sea surface temperatures in the Late Cretaceous and Eocene epochs. *Nature*, **413**, 481–487.
- Peters, K.E.** (1986) Guidelines for evaluating petroleum source rock using programmed pyrolysis. *AAPG Bull.*, **70/3**, 318–329.
- Preto, N. and Hinnov, L.** (2003) Unravelling the origin of carbonate platform cyclothem in the Upper Triassic Dürrenstein Fm. (Dolomites, Italy). *J. Sed. Res.*, **73**, 774–789.
- Reeder, R.J. and Dollase, W.A.** (1989) Structural variation in the dolomite-ankerite solid-solution series: an X-ray, Mössbauer, and TEM study. *Am. Mineral.*, **74**, 1159–1167.
- Reeder, R.J. and Sheppard, C.E.** (1984) Variation of lattice parameters in some sedimentary dolomites. *Am. Mineral.*, **69**, 520–527.
- Riding, R.** (2000) Microbial carbonates: the geological record of calcified bacterial-algal mats and biofilms. *Sedimentology*, **47**(Suppl. 1), 179–214.
- Roghi, G.** (2004) Palynological investigations in the Carnian of the Cave del Predil area (Julian Alps, NE Italy). *Rev. Palaeob. Palyn.*, **132**, 1–35.
- Röhl, H.-J., Schmitt-Röhl, A., Oschmann, W. and Schwark, L.** (2001) The Posidonia Shale (Lower Toarcien) of SW-Germany: an oxygen-depleted ecosystem controlled by sea level and palaeoclimate. *Palaeogr. Palaeoclim. Palaeoecol.*, **165**, 27–52.
- Sageman, B.B., Wignall, P.B. and Kauffman, E.G.** (1991) Biofacies models for oxygen-deficient facies in epicontinental seas: tools for paleoenvironmental analysis. In: *Cycles and Events in Stratigraphy* (Eds G. Einsele, W. Ricken and A. Seilacher), pp. 543–564. Springer, Berlin.
- Scherer, M.** (1977) Preservation, alteration and multiple cementation of aragonitic skeletons from the Cassian Beds (U-Triassic, Southern Alps): petrographic and geochemical evidence. *N. Jb. Geol. Paläont. Abh.*, **154**, 213–262.
- Schlager, W. and Schöllnberger, W.** (1974) Das Prinzip stratigraphischer Wenden in der Schichtabfolge der Nördlichen Kalkalpen. *Mitt. Geol. Ges. Wien*, **66/67**, 165–193.
- Searl, A.** (1994) Discontinuous solid solution in Ca-rich dolomites: the evidence and implications for the interpretation of dolomite petrographic and geochemical data. In: *Dolomites. A volume in honour of Dolomieu* (Eds B. Purser, M.E. Tucker and D. Zenger). *Int. Assoc. Sed. Spec. Publ.*, **21**, 361–376.
- Shinn, E.A. and Robbin, D.** (1983) Mechanical and chemical compaction in fine-grained shallow-water limestones. *J. Sed. Petrol.*, **53**, 596–618.
- Simms, M.J. and Ruffell, A.H.** (1989) Synchronicity of climate change and extinctions in the Late Triassic. *Geology*, **17**, 265–268.
- Simms, M.J., Ruffell, A.H. and Johnson, A.L.A.** (1995) Biotic and climatic changes in the Carnian (Triassic) of Europe and adjacent areas. In: *In the shadow of dinosaurs* (Eds N.C. Fraser and H.D. Sues), pp. 352–365. Cambridge University Press, Cambridge.
- Spötl, C. and Vennemann, T.W.** (2003) Continuous-flow isotope ratio mass spectrometric analysis of carbonate minerals. *Rapid Commun. Mass. Spectrom.*, **17**, 1004–1006.
- Stefani, M., Brack, P., Gianolla, P., Keim, L., Maurer, F., Neri, C., Preto, N., Riva, A., Roghi, G. and Russo, F.** (2004) Triassic carbonate platforms of the Dolomites: carbonate production, relative sea-level fluctuations and the shaping of the depositional architecture. In: *32nd International Geological Congress, Florence, (Italy), Field Trip Guide Book – P44*, 44 pp.
- Steuber, T. and Veizer, J.** (2002) Phanerozoic record of plate tectonic control of seawater chemistry and carbonate sedimentation. *Geology*, **30**, 1123–1126.

- Strasser, A.** and **Davaud, E.** (1983) Black pebbles of the Purbeckian (Swiss and French Jura): lithology, geochemistry and origin. *Ecol. Geol. Helv.*, **76**, 551–580.
- Taylor, J.C.** (1991) Computer programs for standardless quantitative analysis of minerals using the full powder diffraction profile. *Powder Diffract.*, **6**, 2–9.
- Urlichs, M.** (1994) Trachyceras Laube 1896 (Ammonoidea) aus dem Unterkarn (Obertrias) der Dolomiten (Italien). *Stuttgarter Beiträge für Naturkunde, Serie B*, **217**, 1–55.
- Veizer, J., Ala, D., Azmy, K., Bruckschen, P., Buhl, D., Bruhn, F., Carden, G.A.F., Diener, A., Ebner, S., Godderis, Y., Jasper, T., Korte, C., Pawellek, F., Podlaha, O.G. and Strauss, H.** (1999) $^{87}\text{Sr}/^{86}\text{Sr}$, $\delta^{13}\text{C}$ and $\delta^{18}\text{O}$ evolution of Phanerozoic seawater. *Chem. Geol.*, **161**, 59–88.
- Visscher, H., Van Houte, M., Brugman, W.A. and Poort, R.J.** (1994) Rejection of Carnian (late Triassic) “pluvial event” in Europe. *Rev. Palaeobot. Palynol.*, **83**, 217–226.
- Wanless, H.R.** (1979) Limestone response to stress: pressure solution and dolomitization. *J. Sed. Petrol.*, **51**, 437–462.
- Ward, C.R., Taylor, J.C. and Cohen, D.R.** (1999) Quantitative mineralogy of sandstones by X-ray diffractometry and normative analysis. *J. Sed. Res.*, **69**, 1050–1062.
- Wendt, J. and Fürsich, F.T.** (1980) Facies analysis and palaeogeography of the Cassian Formation, Triassic, Southern Alps. *Riv. It. Paleont. Strat.*, **85**, 1003–1028.
- Wright, D.T.** (1999) The role of sulphate-reducing bacteria and cyanobacteria in dolomite formation in distal ephemeral lakes of the Coorong region, South Australia. *Sediment. Geol.*, **126**, 147–157.
- Yin, J., Fürsich, F.T. and Werner, W.** (1995) Reconstruction of palaeosalinities using carbon isotopes and benthic association: a comparison. *Geol. Rundsch.*, **84**, 223–236.

Manuscript received 8 February 2004; revision accepted 14 October 2005